PL-TR-97-2159

ADVANCED GEOPHYSICAL ENVIRONMENT SIMULATION TECHNIQUES – FINAL REPORT

G. B. Gustafson
R. P. d'Entremont
C. F. Ivaldi
S. T. Beresford
D. B. Hogan

Atmospheric and Environmental Research, Inc.
840 Memorial Drive
Cambridge, MA 02139-3794

8 May 1998

Final Report
2 September 1994 – 1 September 1997

19990316 101

AIR FORCE RESEARCH LABORATORY
Space Vehicles Directorate
29 Randolph Road
AIR FORCE MATERIAL COMMAND
HANSCOM AFB, MA 01731-3010

DTIC QUALITY INSPECTED 1

"This Technical Report has been reviewed and is approved for publication"

JOHN CIPAR
Contract Manager

FRANK A. ZAWADA, Lt Col, USAF
Division Director

This report has been reviewed by the ESC Public Affairs Office (PA) and is releasable to the National Technical Information Service (NTIS).

Qualified requestors may obtain additional copies from the Defense Technical Information Center (DTIC). All others should apply to the National Technical Information Service (NTIS).

If your address has changed, if you wish to be removed from the mailing list, of if the addressee is no longer employed by your organization, please notify AFRL/VSOS-IM, 29 Randolph Road, Hanscom AFB, MA 01731-3010. This will assist us in maintaining a current mailing list.

Do not return copies of this report unless contractual obligations or notices on a specific document require that it be returned.

REPORT DOCUMENTATION PAGE

1. AGENCY USE ONLY (Leave blank)	2. REPORT DATE	3. REPORT TYPE AND DATES COVERED
	8 May 1998	Final (2 Sep 1994 – 1 Sep 1997)

4. TITLE AND SUBTITLE

Advanced Geophysical Environmental Simulation Techniques – Final Report

5. FUNDING NUMBERS

PE 35160F
PR 7659 TA GY WU AC
Contract F19628-94-C-0106

6. AUTHOR(S)

G. B. Gustafson, R. P. d'Entremont, C. F. Ivaldi, S. T. Beresford, D. B. Hogan

7. PERFORMING ORGANIZATION NAMES(S) AND ADDRESS(ES)

Atmospheric and Environmental Research, Inc.
840 Memorial Drive
Cambridge, MA 02139-3794

8. PERFORMING ORGANIZATION REPORT NUMBERS

9. SPONSORING / MONITORING AGENCY NAMES(S) AND ADDRESS(ES)

Air Force Research Laboratory
29 Randolph Road
Hanscom AFB, MA 01731-3010

Contract Manager: John Cipar/VSSW

10. SPONSORING / MONITORING AGENCY REPORT NUMBER

PL-TR-97-2159

11. SUPPLEMENTARY NOTES

12a. DISTRIBUTION / AVAILABILITY STATEMENT

approved for public release; distribution unlimited

12b. DISTRIBUTION CODE

13 ABSTRACT *(Maximum 200 words)*

A three-year, multi-faceted effort to develop and apply state-of-the-art techniques for analysis of environmental satellite data is described. Principal accomplishments include development of satellite data analysis and image processing algorithms and software suitable for interpreting environmental satellite sensor measurements; adaptation and application of satellite-based cloud property retrieval algorithms for processing of large multiple-satellite data sets; development and application of improved cloud-phase and cloud optical property retrieval algorithms; investigation of techniques potentially applicable for retrieval of cloud spatial properties from very high resolution remotely sensed data; and data analysis in support of a contrail-formation experiment. Software development and data analysis were performed using the Air Force Interactive Meteorological System (AIMS) located at PL. AIMS is an integrated computer facility that includes multiple direct-broadcast satellite ground stations and associated data processing facilities; an extensive satellite and conventional data archive; a database access system; and a library of environmental-property retrieval algorithms. Several system enhancements were developed for AIMS including a new Geostationary satellite acquisition and analysis capability. All software and data-analysis products developed under this effort are available on AIMS.

14. SUBJECT TERMS

| cirrus | satellite | polar-orbiting |
| cloud retrieval | meteorology | geostationary |

15. NUMBER OF PAGES

16. PRICE CODE

17. SECURITY CLASSIFICATION OF REPORT	18. SECURITY CLASSIFICATION OF THIS PAGE	19. SECURITY CLASSIFICATION OF ABSTRACT	20. LIMITATION OF ABSTRACT
Unclassified	Unclassified	Unclassified	

TABLE OF CONTENTS

LIST OF FIGURES

LIST OF TABLES

1.0 INTRODUCTION

This final report describes a three-year, multi-faceted effort to support the Air Force Phillips Laboratory Data Analysis Division (PL/GPD) in development and application of state-of-the-art techniques for analysis of environmental satellite data. The resulting tools, techniques and data sets support improved analysis of archived data as well as current and future geophysical parameter acquisition and analysis. The principal accomplishments under this contract were:

- software tool and technique development for enhanced satellite image processing and data analysis capabilities on the Air Force Interactive Meteorological System

- adaptation of a set of multi-source, multi-spectral satellite cloud analysis algorithms for processing of large environmental satellite data sets

- application of the cloud analysis algorithms to a series of 10-day, five-satellite data sets acquired over two seasons and at multiple locations around the Earth

- development of improved cloud-phase discrimination algorithms for analysis of GOES imager and AVHRR data

- development of improved algorithms for retrieval of cirrus emissivity and estimation of cloud altitude

- application of existing cloud detection and new cloud-phase and emissivity algorithms to a two-month data set collected from one GOES and two NOAA satellites over the eastern and central portions of the continental U.S. and western Atlantic

- investigation into the variability of retrieved cloud spatial properties when remotely sensed at varying spatial resolution reduction

- quality assurance processing of approximately one month of raw radiosonde data from five sites in support of a contrail experiment.

All software development, data processing, and analysis were performed on the Air Force Interactive Meteorological System (AIMS) located at the Air Force Phillips Laboratory Atmospheric Sciences Division (I L/GPA) facility at Hanscom Air Force Base. AIMS is an integrated facility consisting of multiple real-time meteorologicalsatellite ground receiving stations, a comprehensive archive of satellite and conventional data products, a database access system, a set of state-of-the-art algorithms for satellite data analysis, and a hybrid computing environment. AIMS is jointly operated by the US Air Force and Atmospheric and Environmental Research, Inc. (AER) under the terms of a Cooperative Research and Development Agreement (CRADA).

Cloud-analysis related algorithm development built on an existing set of satellite analysis algorithms developed under earlier programs at the Phillips Laboratory. The key research project codes are:

- TACNEPH (contract # F19628-90-C-0112): basic cloud properties (cover, layers, type) for DMSP and NOAA satellites as appropriate for processing in a military tactical environment;

- SERCAA Phase I (contract # F19628-92-C-0149): basic cloud properties (cover, layers, type) for both polar-orbiting (DMSP and NOAA series) and geosynchronous (GOES, GMS and METEOSAT) satellites plus an analysis integration processing step which produces a single optimal synoptic analysis from all available multi-satellite data sources;

- SERCAA Phase II (contract # F19628-92-C-0149): enhanced cloud properties including cirrus properties (emissivity, effective height and effective temperature), cloud phase, and integration of cloud analysis with microwave sounding.

Adaptation and application of SERCAA, Phase I, cloud algorithms was performed in support of a Defense Nuclear Agency (DNA) cloud-forecast development program. Cirrus algorithm development, data analysis work, and algorithm comparison studies supported the Backgrounds Working Group of the of the Space Based Infrared System (SBIRS) Phenomenology Exploitation Project. Cloud spatial-property investigations were conducted in support of the MEDEA project. Radiosonde data processing was in support of a Phillips Lab project to investigate conditions conducive to contrail formation.

This report is organized as follows. Section 2 summarizes the AIMS facility and advancements made over the course of the contract; Section 3 describes the required adaptation of the SERCAA Phase I algorithms to process the DNA data sets and provides an overview of the data sets produced for DNA; Section 4 summarizes the cloud phase and cirrus retrieval algorithm development and discusses work to generate large-volume data sets in support of the SBIRS Phenomenology Exploitation Project; and Section 5 describes the reduction and quality assurance work on the radiosonde data collected for the contrail program.

2.0   AIR FORCE INTERACTIVE METEOROLOGICAL SYSTEM (AIMS)

The Air Force Interactive Meteorological System (AIMS) is an integrated system composed of general-purpose and function-specific processors developed originally to support research in remote sensing, principally satellite meteorology. AIMS is jointly operated and maintained by PL/GPA and AER under a Cooperative Research and Development Agreement (CRADA). Over the course of the contract, AIMS underwent considerable down-sizing as aged and redundant systems were replaced by improved equipment. Numerous enhancements to both the software and hardware capabilities of the system were also introduced. Figure 1 provides a schematic of the AIMS components at the start of the contract and Figure 2 identifies the current system components. Table 1 provides a functional description of the AIMS components.

AIMS was designed to support research in satellite meteorology through five functional capabilities: network access; real-time and archived data sources; data visualization and image processing; interactive and batch processing; and high capacity online storage. Ethernet hardware provides the network backbone for AIMS, all systems are either tied directly to the AIMS Ethernet or are reachable through a network gateway computer. The UNIX-based platforms (SGI and SUN) share data directly using SUN Microsystems Network File System (NFS) while a third-party implementation of NFS, known as MultiNET, allows the Alpha processor to participate in the local-area network as an NFS client and server. The PL laboratory network links the AIMS through an Ethernet bridge to outside networks including NSI, DDN, and NEARnet (DDN and NEARnet are both members of Internet) thereby providing access to laboratories, government facilities, and private companies world wide.

Meteorological and supporting data flow into AIMS through several possible routes: 1) real-time direct broadcast satellite transmissions, 2) direct serial links, 3) 9 track, 8 mm, or 4 mm DAT magnetic tape, 4) network file transfers (e.g., FTP), or 5) CD ROM optical disks. Satellite transmissions are received directly at one of four satellite ground stations configured to receive GOES, NOAA/HRPT, METEOSAT, and DMSP broadcasts. Table 2 summarizes the characteristics of the sensor data routinely ingested by these systems. Satellite coverage is restricted to direct line-of-sight from the AIMS ground stations. Figure 3 shows the coverage area available from polar-orbiting and geostationary platforms. GOES, NOAA/HRPT, METEOSAT and DMSP ground station computers use a comprehensive third-party software package known as Terascan used to extract, format, calibrate, and Earth-locate the telemetry

data. X11 windows-based software is also provided for interactive image display and processing of the data. All routinely scheduled data ingest events from the four ground stations are archived either to 4mm or 8mm tape. Table 3 summarizes the regional satellite data archive on AIMS.
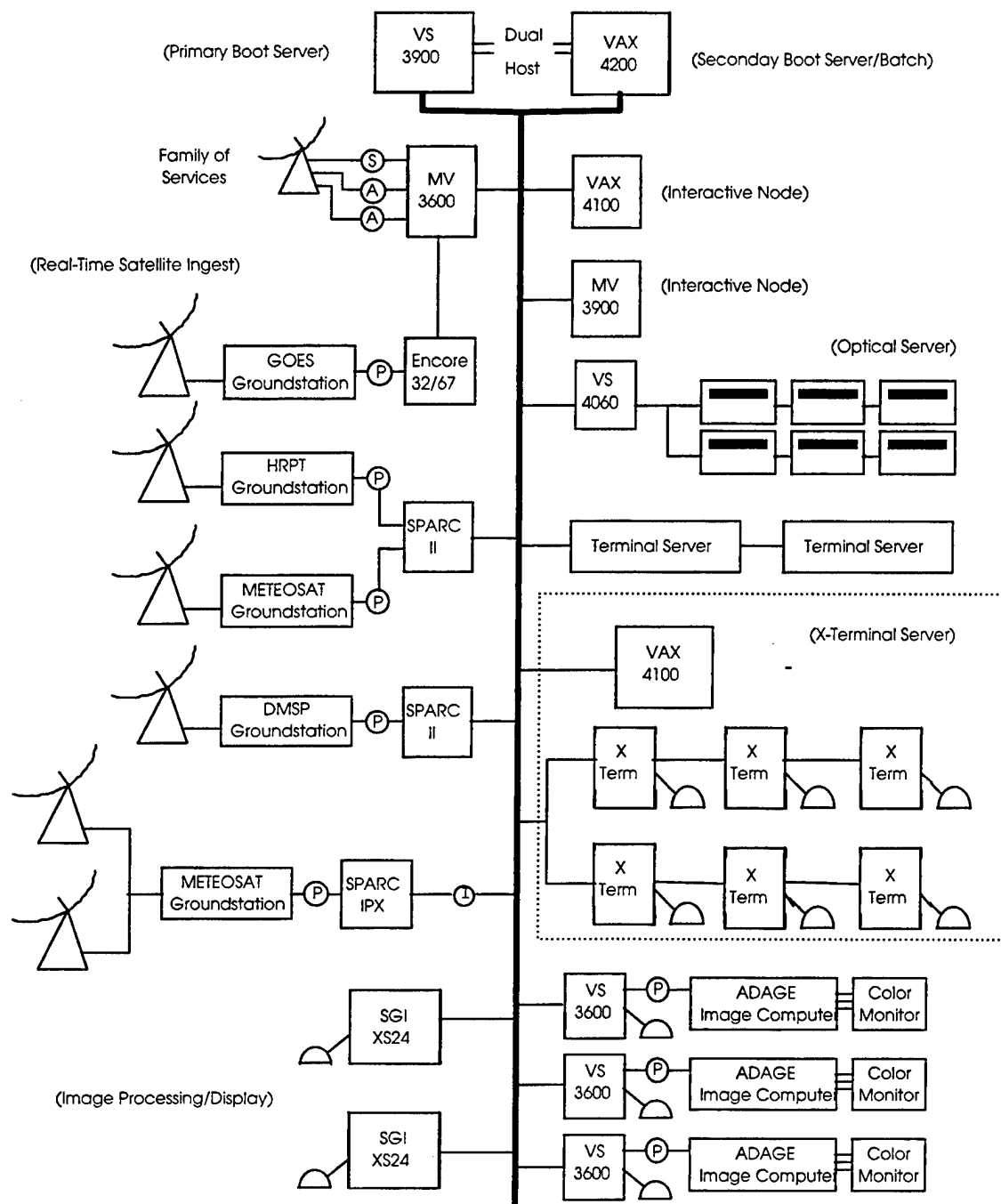
Figure 1 AIMS configuration at initiation of program
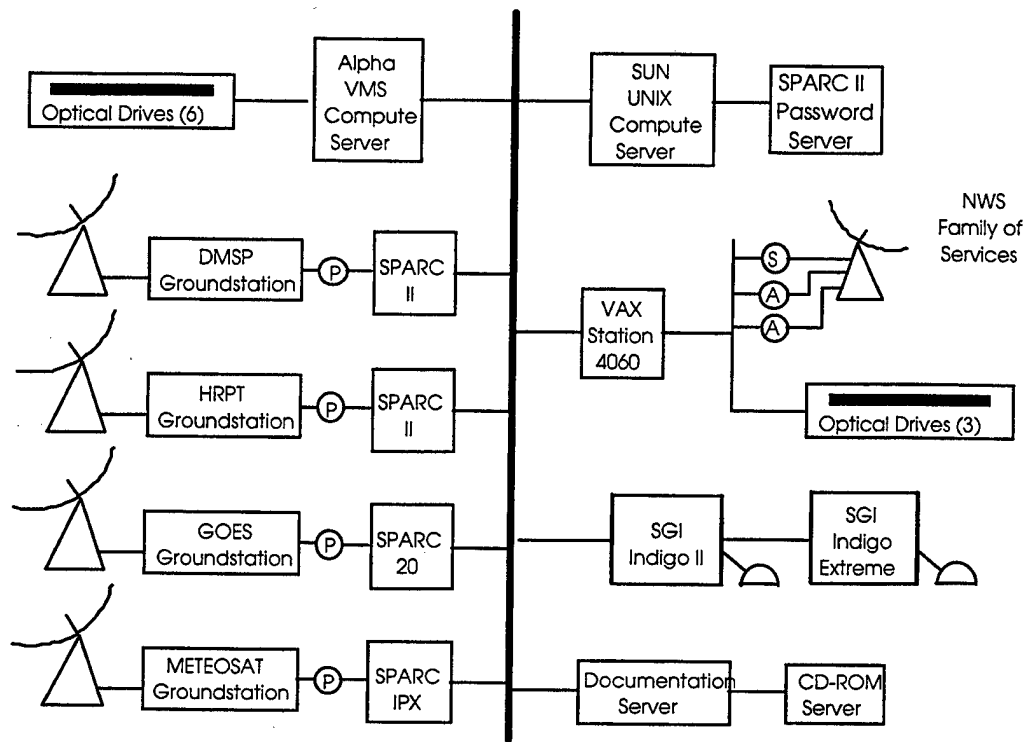
Figure 2 AIMS configuration at conclusion of program

Table 1 Physical and functional overview of AIMS components

Qty	System	O.S.	Memory (MB)	Disk (GB)	Tape	Description
1	Sun Sparc 20	UNIX	64	7	8mm	GOES-8/9 real-time ingest
1	Sun Sparc II	UNIX	64		4mm	NOAA/HRPT real-time ingest
1	Sun Sparc II	UNIX	64	2.4	4mm	DMSP/RTD real-time ingest
1	Sun Sparc IPX	UNIX	64	5	4mm	METEOSAT-5 real-time ingest
1	Silicon Graphics Indigo2 Extreme	UNIX	96	3		Image processing/display
1	Silicon Graphics Indigo Extreme	UNIX	128			Image visualization Software development
1	Micron PC	WINT	64		8mm 1/4	Intranet documentation server
1	Micron PC	W/95	64		1/4	CD-ROM server
1	AlphaServer 2000	VMS	256	8	8rnm	Oracle database server
1	Sun Enterprise 2	UNIX	576	12	8mm	Compute server
	VAXstation 4060	VMS	72	2.5		8-bit image display Weather data ingest

Table 2 Instrument characteristics for sensor data available from AIMS

Satellite/Channel	Instrument Wavelength or Frequency	Nadir Resolution (km)
DMSP OLS		
Visible	0.4 - 1.1 μm	0.6
Longwave IR	10.5 - 12.6 μm	2.8
DMSP SSM/I		
1	19.35 GHz V/H	25
2	22.235 GHz V	25
3	37.0 GHz V/H	25
4	85.5 GHz V/H	12.5
DMSP SSM/T2		
1 (Window)	91.5 GHz	90
2 – 5 (H$_2$O)	150 GHz, 183 +/- 1 GHz, 183 +/- 3 GHz, 183 +/- 7 GHz	64
NOAA AVHRR		
1	0.58 - 0.68 μm	1.1
2	0.725 - 1.1 μm	1.1
3	3.55 - 3.93 μm	1.1
4	10.3 - 11.3 μm	1.1
5	11.5 - 12.5 μm	1.1
NOAA HIRS		
1 - 7 (CO$_2$/H$_2$O)	13.3, 13.6, 13.9, 14.2, 14.4, 14.7, 14.9 μm	42
8 (Window)	11.11 μm	42
9 (O$_3$)	9.71 μm	42
10 - 12 (H$_2$O)	6.72, 7.33, 8.22 μm	42
13 - 17 (N$_2$O/CO$_2$)	4.23, 4.40, 4.46, 4.52, 4.57 μm	42
18 - 19 (Window)	3.76, 4.00 μm	42
20 (Window)	0.69 μm	42
NOAA MSU		
1 (Window)	50.31 GHz	168
2 – 4 (O$_2$)	53.74 GHz, 54.96 GHz, 57.95 GHz	168
GOES Imager		
1	0.55 – 0.75 μm	1
2	3.8 – 4.0 μm	4
3	6.5 – 7.0 μm	8
4	10.5 – 11.2 μm	4
5	11.5 – 12.5 μm	4
GOES Sounder		
1-7 (CO$_2$/H$_2$O)	14.71, 14.37, 14.06, 13.64, 13.37, 12.66, 12.02 μm	8
7-8 (Window)	12.02, 11.03 μm	8
9 (O$_3$)	9.71 μm	8
10 – 12 (H$_2$O)	7.43, 7.02, 6.51 μm	8
13 – 16 (N$_2$O/CO$_2$)	4.57, 4.52, 4.45, 4.13 μm	8
17 – 19 (Window)	3.98, 3.74, 0.70 μm	8
METEOSAT		
1	0.5 – 0.9 μm	2.5
2	5.7 – 7.1 μm	5
3	10.5 – 12.5 μm	5

(a)   (b)

Figure 3 (a) Line-of-sight polar satellite coverage area; (b) Direct broadcast geostationary coverage area

Table 3 Duration of AIMS direct-broadcast satellite data archive

Platform	Duration
NOAA-11/12/14	22Sep92 - present
DMSP-F1 l/F12	1Sep93 - present
GOES-8/9	28Jul95 - present
METEOSAT-4/5/6	15Sep93 - present

Conventional meteorological data are used extensively on AIMS to support various applications. These data are made available via serial connections to two components of the National Weather Service (NWS) Family of Services. The first component, known as the Domestic Data Service (DDS), provides coded observations, reports, forecasts, and analyses for the U.S., Canada, and the Caribbean. The second component is known as the International Data Service (IDS) and provides worldwide coded observations, reports, and forecasts. The Family of Services multiplexes data originating from different sources, producing a data stream of point, gridded, and tabular data with varied formats. AIMS recognizes, decodes and reformats a subset of data sources that includes Service A, synoptic, ship and buoy, METAR, upper-air, manually digitized radar (MDR), and NMC model guidance. Table 4 describes the conventional meteorological data sources available on AIMS. All data have been archived to 8mm tape since September of 1989.

Table 4 Conventional Meteorological Data Sources Available on AIMS

Source	Type	Coverage	Frequency	Data Characteristics
Service A[1]	Point	US, Canada	Hourly	Surface observations
Synoptic	Point	Global	4/8 times daily	Surface observations
METAR	Point	Global	8 times daily	Surface observations
Ships/Buoys	Point	Global	4/8 times daily	Platform observations
Upper Air	Point	Global	Twice daily	Radiosonde measurements
Forecast Guidance	Point	US	Twice daily	ETA and NGM model output. Forecasts for 6 hour intervals out to 48 hours
Forecast Model Output Statistics (MOS)	Point	US	Twice daily	Statistically-based forecasts derived from the models. Forecasts for 6 hour intervals out to 48 hours
Trajectory Forecasts	Point	US	Twice daily	Statistically-based forecasts derived from the models. Includes parcel trajectories for 6 hour intervals out to 24 hours
Manually Digitized Radar (MDR)	Gridded	US	Hourly (on the half-hour)	Maximum reflectivity reported for grid box. Also station status and some cell characteristics

[1]On July 1, 1996 the Servic A format was changed to METAR.

Data on magnetic tape are received from numerous outside agencies including AFGWC, ETAC, NOAA/NESDIS, NASA, NCAR, ASL and GMGO. Historically, tapes have been the preferred method for transferring data from outside the organization; however, this has been replaced by direct file transfers via Internet. Most network file transfers from outside the laboratory enter the system via a separate gateway computer maintained by the Geophysics Directorate's main computing center. This gateway computer is a node on the GP network and communicates with AIMS using various protocols, most notably the TCP/IP protocol. Recently, the Defense Mapping Agency began distributing large volume geographic data sets on CD ROM. CD ROM is also becoming the preferred medium for soflware vendors to distribute new and revised software packages to customers.

Satellite data dominate all other data types in competition for system resources. A primary system design consideration for AIMS was effective management of the large amount of imager and sounder data available from the satellite sensors (see Table 2) as well as products derived from the raw data (e.g., algorithm development for cloud analysis and forecasts). To this end, a DEC Alpha running an Oracle Database Server, a networked-based relational database management system, was configured to facilitate management and user access to the vast amount of archived and online satellite data. AIMS currently supports 64GB of fixed disk mass storage as well as rewritable optical disk drives that provide 1.3GB of storage per cartridge. With nine

optical drives currently configured on AIMS, 5.4GB of data can be made immediately available at any one time. Fixed disk mass storage is routinely backed-up to 8mm tape.

Visualization of data and experiment results is arguably the single most important capability on AIMS. Virtually every scientific project that uses AIMS exploits this capability, at least for quality control of the input data and validation of algorithm results. There are basically two types of display systems on AIMS. The first type is the two SGI Indigo imaging workstations. These workstations extend the visualization capabilities of AIMS through a high performance RISC-based workstation capable of real-time 2- and 3-D graphics and imaging that can be implemented using standards such as the X Windows system for 2-D applications and OpenGL for 3-D graphics and imaging. The SGI systems have 224 MB of system memory that doubles as pseudo frame buffer memory and a 7 GB of online image storage. Vendor supplied software includes Explorer, interactive visualization software for 2- and 3-D applications and ImageVision, an objectoriented library used to create, process, and display imagery. Work during the contract focused efforts to port much needed application functionality from older Adage systems to the SGI systems. The third type of display system available on AIMS are desktop color X-terminals. These systems are characterized by 8-bit color graphics, ample system memory, and host services provided by SUN, SGI, or DEC platforms. They provide an X window based interface to AIMS, support local clients including TELNET, CTERM and LAT services, generally reside within individual offices and are used for a variety of applications including software development, analysis and display of meteorological data, word processing, network communications, and other general purpose computing. X windows is the *de facto* interface standard for all AIMS workstations due to its functionality and nearly universal acceptance across hardware platforms.

Although AIMS was primarily developed to support interactive computing, there has been a consistent secondary need to support computer intensive jobs through batch processing. A DEC Alpha and a SUN Enterprise 2 multi-processor system were added to AIMS to provide a strong batch processing capability. Legacy software is generally run on the Alpha system since historically most software development was done in a VMS environment. Most new software development is being done on UNIX systems, and the Enterprise server was acquired to address the needs of these users.

Software has been developed on AIMS to perform standard display operations for satellite imagery such as gray shade imaging, pseudo color enhancements, time-series looping and

9

graphical display. The SGI systems support full color display of multispectral imagery as well as fast interactive image enhancement and filtering operations. The Image Vision library provides a core set of image processing functions that include color conversion, arithmetic functions, radiometric and geometric transforms, statistics, spatial and non-spatial domain transforms, and edge, line, and spot detection. For conventional meteorological data, a substantial number of applications have been developed to facilitate access to and processing of these data. General purpose list, plot, and contour applications are available for use. Data access methods supported by these applications include time-series for a single station; geographic retrievals by station list, political boundary, latitude-longitude box, or user-defined keyword; and compound retrievals for data fusion applications. For applications development, AIMS supports the C, C++, and FORTRAN languages for 3GL programs; IDL, GKS, NCAR Graphics, MOTIF/X11, Explorer, OpenGL, and ImageVision for graphics and imaging and X-Designer for building graphical users interfaces.

Other resources available on AIMS include a dial-in capability (2 lines), black and white and color laser printers and a high-quality color printer based on dye-sublimation technology suitable for producing publication-quality hard copy output. A Pentium-based PC running the Windows NT-Server operating system acts as an Intranet documentation server, providing documentation for programmed applications and libraries, computer-related procedural tasks (e.g. how to restore selected archives), and file format descriptions to name a few. Users seeking documentation will be able to use a web browser to query and locate specific documentation from the server. A second Pentium-based PC hosts a CD-ROM Recorder for creating CD-ROMS and a 2GB user disk to stage recording data. The PC is networked so that users can transfer data from any AIMS node to the staging disk using FTP or NFS.

2.1   AIMS SATELLITE GROUND STATIONS

As discussed above, AIMS includes four satellite ground stations for acquisition and processing of direct-broadcast data from NOAA-TIROS, DMSP, METEOSAT, and GOES satellites. During the contract period, the US launched the first in a new series of geosynchronous weather satellites known as GOES-NEXT. The first satellite of the new series, GOES-I, was launched on April 14, 1994 and, after completing a period of engineering tests and an operational demonstration phase, became operational on June 11, 1995 and was designated GOES-8. The next satellite in the GOES-Next series, GOES-J, was launched on May 23, 1995 and was placed in operational status on January 22, 1996 with a designation of GOES-9.

GOES-Next satellites have a different and dramatically more-capable sensor payload than the previous GOES-series as well as a new data format termed GOES Variable (GVAR). For the AIMS system to maintain currency, and to provide the state-of-the-art satellite data sets, AER was directed by the government to review alternatives to upgrade the system for acquisition and processing of GOES-8 and GOES-9 direct broadcast data.

Two approaches to achieving a GOES-8 capability were evaluated. The first relied on the existing system that included an 8-meter tracking antenna, Aydin 1050 subsystem (demodulator, bit sync and frame sync), and an Integral Systems Downlink Interface. The ground station computer was a nine year old Encore 3/67 minicomputer running the MPX-32 real-time operating system. While the antenna had ample gain to receive the high quality GOES-NEXT data stream, this approach presented a number of problems. Some system components were over 20 years old and contained obsolete equipment in both the RF chain and for the antenna mechanical systems. The processing software for the controlling computer was developed in-house and not readily upgraded to GOES-NEXT. Pursuing this approach would have required the following:

- extensive software development to either upgrade the existing software for GOES-NEXT or to interface it to a third-party software product
- uncertain number of engineering hours to work each of the components in the RF chain and make the necessary changes including feed assembly, bitsynchs, and frame-synchs
- severe risk of a major mechanical failure which could not readily be repaired due to parts obsolescence.

The alternative approach was to modify an existing METEOSAT ground station. This system was receiving data from the ME EOSAT-3 satellite which was then positioned over the central Atlantic Ocean. These data would be made largely redundant by GOES-8 and thus no longer needed when data from the new satellite were available. The METEOSAT ground station had been recently manufactured and was still fully supported by the vendor with none of the parts obsolescence problems of the first alternative. The following modifications were required to convert the system:

- a new LNA, feed
- new down-converter
- new bit synchronizer
- reprogram the METEOSAT frame synchronizer
- upgrade the METEOSAT Sparc IPX workstation

11

- move the METEOSAT antenna (which was located at AER's Cambridge facilities) and install on the roof of the Phillips Laboratory (GPAB)
- complete integration and testing at Hanscom AFB.

A quote was received from the ground station vendor, Seaspace Corporation, to perform the above tasks except for the move and reinstallation of the antenna for which a separate quote was obtained. AER reviewed these alternatives with the government, who concurred with our recommendation of proceeding with the second approach: modification of the METEOSAT ground station.

A secondary issue emerged concerning the high data rate and volume of GOES-NEXT broadcasts. It was unclear whether the existing Sparc IPX was capable of handling the data acquisition, Earth location, and calibration functions while simultaneously providing an interactive data analysis capability. An interim solution was identified to perform the data analysis functions on the underutilized DMSP ground station computer. This approach incurred no additional costs, but still presented potential processing conflicts. A preferred long term solution to acquire another Terascan License for one of the SGI Indigo workstations was suggested. This would enable off-line post processing and value added processing to occur on a high end workstation, well-suited to the large volumes of GOES-NEXT data. Ultimately, the issue was resolved through the acquisition of a high-end SPARC-20 workstation as the GOES ground station computer.

In July of 1995 AER contracted with Seaspace to upgrade the METEOSAT-3 ground station to make it GOES-NEXT capable. The purchase of the GOES system from Seaspace maintained a consistent base of weather satellite processing systems, allowing computer hardware and software to be easily integrated into the existing computer network. It also provided consistency in vendor-supplied software to ingest and process weather satellite data that scientists and support personnel are already familiar with.

The GOES-8 system technical specifications are as follows:

ACQUISITION ELECTRONICS:
- Paraclipse 12' antenna, LNA and downcon
- Seaspace HR100 receiver/bit synchronizer
- Seaspace S-BUS frame synchronizer

COMPUTER HARDWARE:
- SUN Sparcstation 20 with:
    64 MB system memory
    1 GB system disk

4 GB user disk
Two 1GB pass disks
CD-ROM drive
8mm stacker

COMPUTER SOFTWARE:
- Solaris 2.4 operating system
- Terascan 2.6 satellite ingest and processing software

The following chronology summarizes the GOES-8 ground station installation/integration:

3/95: final purchase orders placed

4/95: Sparc IPX memory and disk upgrades made; Sparc shipped to Seaspace for system integration

5/95: METEOSAT antenna moved from Cambridge to PL/Hanscom

7/95: Seaspace complete integration and testing at their facilities and ships equipment

7/95: system installed and tested at PI /Hanscom; basic operating capability demonstrated

8/95: regular archiving of GOES-8 data initiated

2.2 GOES-NEXT DATA PROCESSING

The GOES-8 satellite is positioned in a geostationary orbit at 75 degrees west longitude. GOES-9 is located at 135 degrees west longitude. General imaging operations occur on a repeating half-hour schedule beginning at 15 and 45 minutes past the hour for GOES-8 and on the hour and half hour for GOES-9. In the routine mode of operation, the satellites view the full northern hemisphere, continental US (CONUS) most of the southern hemisphere. Once every three hours the satellites view the full Earth disk. Table 5 shows the geographic extent of the sectors used in the GOES-8 operations while Figure 4 illustrates how these frames fit into the operational schedule. Note the five half-hourly cycles comprised of the extended northern hemisphere, CONUS, and southern hemisphere (small sector) frames that divide the three-hourly full disk cycle. Similar information for GOES-8 sounder operations is shown in Table 6 and the lower half of Figure 4.

Table 5 Geographical definitions for GOES-8 imaging frames

Sector	Boundaries			
	North	South	West	East
Full Disk	Earth Edge			
Full Disk – Abbreviated	90° N	51° S	Earth Edge	
Full Disk	90° N	23° S	Earth Edge	
Northern Hemisphere	66° N	2° N	117° W	36° W
Northern Hemisphere-Extended	66° N	20° S	117° W	36° W
Southern Hemisphere-South	20° S	50° S	117° W	36° W
Continental US (CONUS)	61° N	14° N	111° W	62° W
Southern Hemisphere-Small Sector	0°	15° S	114° W	81° W

Table 6 Geographical definitions for GOES-8 sounding frames

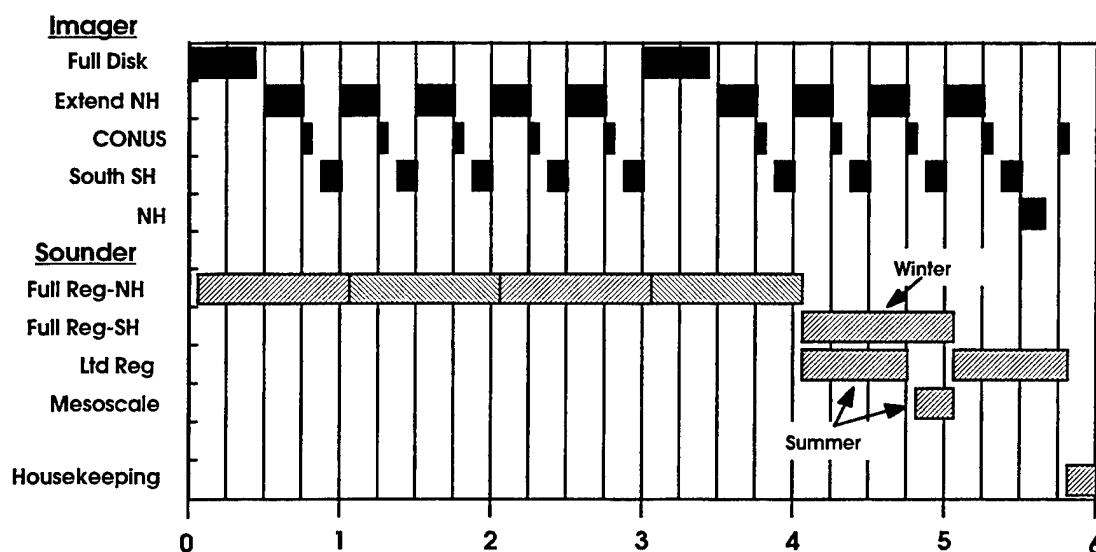| Sector	Boundaries			
	North	South	West	East
Full Regional-NH	51° N	23° N	121° W	64° W
Limited Regional-NH	50° N	26° N	120° W	66° W
Full Regional-SH	22° N	50° S	121° W	64° W
Meso-Tropics 4	23° N	11° N	115° W	93° W

Figure 4 Routine mode operational schedule for GOES-8 imaging and sounding

The GOES-NEXT ground station system has been configured so that real-time acquisition software runs continuously, allowing all frames broadcast by the satellite to be detected and

14

processed. The software stores all data from the telemetry stream to one of four partitions configured over two disks (known as pass disks). Data stored on these partitions are volatile since they are used in a round-robin fashion, driven by each satellite frame detected in the broadcast stream. Typically, once a frame has been completely ingested, post-processing software is activated to extract sensor and ancillary data, format the data, and archive it to 8mm tape. An alternative to processing data from disk is to process the data in real-time as it is received. This is a new capability that allows one or more user-generated scripts to be executed during data acquisition. A script will contain commands that specify the geographic extent, spatial and spectral resolution, and engineering units of the data. Scripts can also contain UNIX commands for performing post-processing activities such as data compression and data archive. The advantage of processing data in real-time (versus dumping the raw data to disk) is that once ingest is complete for a frame or a user-defined subset, the data are immediately available for use. With data first going to pass disks, the user must wait for the entire frame to be acquired before ingest software can be run to reformat the data from the raw stream. As an example, a user-defined subset describing CONUS could be extracted from an extended northern hemisphere frame and be made available for use seven minutes after the start of the frame. The same subset would not be available until 17 minutes after the start of frame if processed from a pass disk partition.

The GOES-NEXT imaging sensor focal plane components include eight visible channel detectors linearly aligned in the north-south direction that are sampled simultaneously and digitized to 10-bit words with a nominal resolution of 1 km square at nadir. Seven thermal detectors of two different sizes sense infrared radiation in four spectral channels. Three of the channels, 3.9, 10.7 and 12.0 μm central wavelength, employ small detector pairs that are simultaneously sampled and digitized to 10-bit words with a nominal resolution of 4 km square at nadir. The 6.75 μm channel employs the large detector, also providing 10-bit data with a nominal resolution of 8 km square at nadir. All IR detectors have redundant counterparts.

Beginning in August 1995, the AIMS GOES-NEXT ground station has routinely acquired and processed half-hourly extended northern hemisphere sectors containing GOES-8 data from all five channels. These data are then automatically formatted as UNIX tar files and written to 8 mm tape as part of the routine AIMS data archive process. Data are Earth located and calibrated. IR data are stored at their full spatial resolution as brightness temperatures while visible data are

15

sub-sampled to match the lower 4 km IR resolution and stored as scaled percent albedo. Data quality has generally been excellent with little or no line dropouts.

3.0 DNA WORLDWIDE SATELLITE DATA SETS

Substantial changes in the operational satellite cloud analysis methodology in use at the Air Force Global Weather Central (AFGWC) will occur as a result of the ongoing Cloud Depiction and Forecast System (CDFS) II upgrade program. The existing cloud analysis model, known as RTNEPH (Real-Time NEPHanalysis), will be replaced by a new model based on a series of algorithms developed by AER under contract to the Air Force Phillips Laboratory (PL) through support from the Strategic Environmental Research and Development Program (SERDP). The new cloud analysis model is referred to as the Support of Environmental Requirements for Cloud Analysis and Archive (SERCAA) model (Gustafson et al., 1994). In addition to cloud analysis, CDFS II will also implement a new cloud forecast model. However, the CDFS II forecast model is a combination of previously existing models that provides no new science. In response to this perceived deficiency, the Defense Nuclear Agency (DNA) conducted an independent research effort to develop and test a new cloud forecast model capable of generating both short and long-term forecasts. To support the forecast model development effort, DNA funded work under this contract to generate SERCAA data products for use in initializing and testing the new forecast models. SERCAA data products were selected to provide compatibility with the cloud analysis products that will eventually be produced by CDFS II.

3.1 SERCAA CLOUD ALGORITHMS

SERCAA algorithms provide for integration of sensor data from both military and civilian polar orbiting environmental satellites plus high temporal resolution imagery from geostationary platforms. The use of high spatial, spectral, and temporal resolution multispectral data obtained from multiple satellite systems is a major innovation over the existing cloud model. RTNEPH is constrained to operate using two-channel data from polar orbiting satellites maintained at degraded spatial and spectral resolution in the AFGWC Satellite Global DataBase (SGDB). SGDB is limited to single visible and infrared channel data from either DMSP or, when DMSP data are unavailable, NOAA polar orbiting operational satellites. Further, AFGWC employs a remapping process to warp the sensor data to a standardized polar stereographic map projection with a concomitant reduction in spatial resolution from 2.7 km to approximately 6 km. Radiometric resolution is also reduced from 8 (DMSP) or 10 (NOAA) bits to 6 bits (i.e., 64 discrete values), resulting in a thermal resolution of infrared brightness temperatures of approximately 1.9 K.

SERCAA algorithms operate on calibrated sensor data at the full spatial and spectral resolution of the sensor (Table 7). In addition to two channel DMSP/OLS data, multispectral NOAA/AVHRR and hourly geostationary data from GOES, GMS, and METEOSAT are also processed. To best exploit the information content from each sensor, and to minimize distortion of the data, cloud analysis is performed in the raw satellite scan projection using all available data bits. No remapping or truncating of the pixel data occurs. To accommodate this approach, sensor data from the individual satellite systems are analyzed separately using multiple analysis algorithms each designed to exploit the unique sensor data attributes of a particular satellite system. The analysis algorithms are organized into four processing layers as illustrated in Figure 5. The first layer employs data ingest code for each satellite system. The second consists of the three satellite specific analysis algorithms, one each for OLS, AVHRR, and geostationary data. These algorithms provide cloud location information on a pixel-by-pixel basis. The third layer further analyzes regions classified as cloud to provide information on the vertical distribution of cloud layers including number, height, and type. Cloud layer information is accumulated over a standard AFGWC 16th mesh (24 km) polar grid. The final processing layer analyzes total cloud and layer information derived from the separate satellite specific algorithms to produce a single integrated cloud analysis. The integration algorithm uses a rules-based approach combined with a modified optimal interpolation scheme to account for differences in timeliness and accuracy characteristics in the separate, asynchronous cloud analyses produced by the earlier processing layers. Final integrated cloud products are total cloud amount plus amount, height, and type for each cloud layer.

The CDFS II cloud model will operate following the steps in the data flow diagram in Figure 5. Acquisition of new satellite data from either a polar or geostationary satellite will trigger processing layers 1-3 to ingest the raw data, perform pixel-level cloud detection, and comput layer statistics. Results from each satellite are stored separately in a local database. The second stage will be a schedule driven operation wherein the final cloud analysis will be produced through integration of the most timely satellite analyses available in the local database. A global integrated cloud analysis will be produced hourly and stored in a central database on the AFGWC 16th mesh grid.

Table 7 Sensor channel attributes of data used in DNA study

Satellite	Sensor	Channel (μm)	Data Format	Resolution[1] (km)	Bits per Pixel[2]	Pixels per Scan Line
DMSP	OLS	0.40-1.10	counts	2.7	6	1464
		10.5-12.6	EBBT	2.7	8	1464
NOAA	AVHRR	0.58-0.68	percent albedo	4.0	8	409
		0.72-1.10	percent albedo	4.0	8	409
		3.55-3.93	EBBT	4.0	8	409
		10.3-11.3	EBBT	4.0	8	409
		11.5-12.5	EBBT	4.0	8	409
GOES	VAS	0.55-0.75	counts	0.9	6	15288
		3.71-4.18	EBBT	14.0	8	1911
		10.5-12.6	EBBT	7.0	8	3822[3]
METEOSAT	VISSR	0.55-0.75	counts	2.5	8	5000
		10.5-12.6	EBBT	5.0	8	2500
GMS	VISSR	0.5-0.75	counts	1.25	6	10000
		10.5-12.5	EBBT	5.0	8	2500

[1]sensor resolution at satellite subpoint

[2]AVHRR radiance data are transmitted at 10-bit resolution, however, the SERCAA development system could only accommodate 8-bit brightness temperature data (although the full 10-bit resolution is used in the radiance to brightness temperature transformation)

[3]GOES long wave infrared data are over sampled in the across-track direction by a factor of 2.
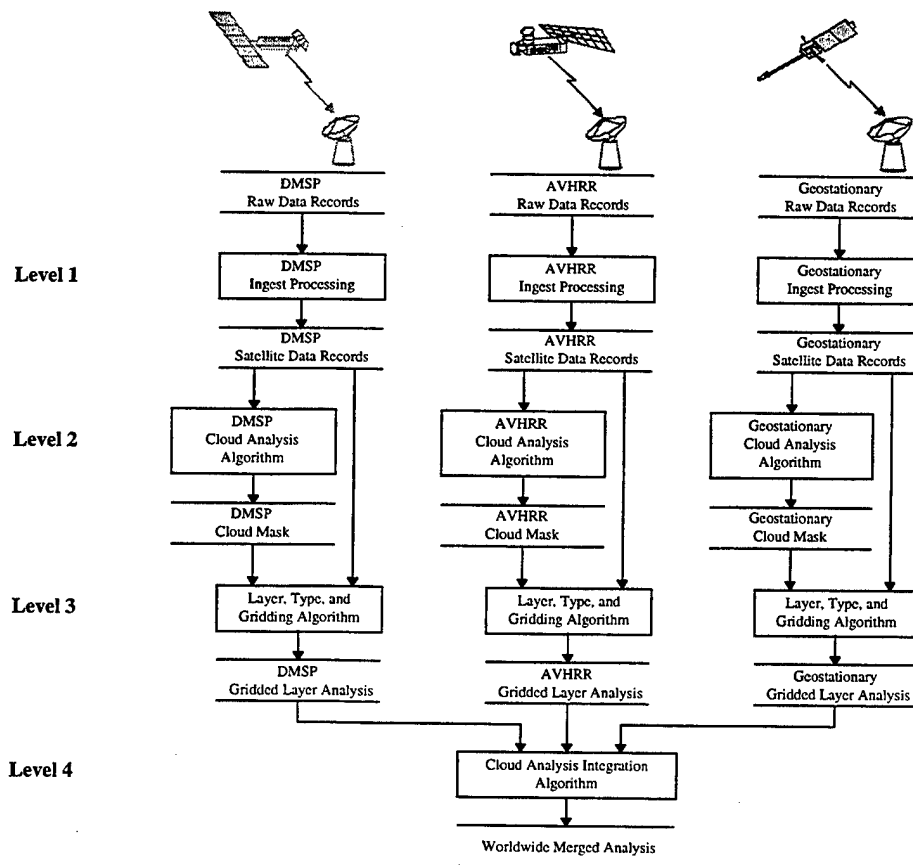

Figure 5 SERCAA/CDFS II-nephanalysis processing flow

The CDFS II cloud model is expected to provide more accurate analyzed cloud products relative to the RTNEPH. The respective characteristics of the RTNEPH vs. the CDFS II cloud model are summarized in Table 8. It is well established that the RTNEPH is deficient in the tropics due largely to strong diurnal variations in cloud amount not captured in the periodic coverage available from polar satellites. This problem is made worse by the timing of the early morning/evening DMSP passes which, when persisted, generally become out of phase with cloud amount trends. Use of geostationary data will greatly increase temporal resolution, particularly in the tropics where polar coverage is poorest and geostationary coverage is best. Similarly, use of multiple polar satellites (i.e., both civilian and military) will increase temporal coverage for all areas of the globe. Improved cloud detection accuracy from analysis of five channel AVHRR data, relative to two channel OLS data, is also expected. SERCAA algorithms exploit AVHRR multispectral data content to address a number of specific problem areas in the RTNEPH: detection of thermally-indistinct low cloud, snow/cloud discrimination, classification of optically thin cirrus, over-analysis along coastlines and over deserts, and sun glint/cloud discrimination. Use of the full spectral resolution of the OLS data will also increase sensitivity to clouds that exhibit weak thermal signatures. Simply by using all 8 bits available from the IR sensor, granularity of derived brightness temperatures increases from 1.9 to 0.5 K. Analysis of sensor data in raw satellite scan projection will minimize distortion caused by warping and truncation of data resulting in fewer analyzed cloud features that are in reality artifacts of the remapping process (e.g., over analysis near coastlines caused by inaccurate geo-location of satellite data).

Table 8 Characteristics of CDFS-II cloud model and RTNEPH

Attribute	CDFS-II Cloud Model	RTNEPH
Spatial resolution	16th mesh (24 km)	8th mesh (48 km)
Global update frequency	1 hour	3 hours
Number of satellites	9 – polar and geo	2 – polar only
Sensor data	DMSP – OLS NOAA/TIROS – AVHRR GOES, METEOSAT, GMS	DMSP – OLS[1]
Algorithm	Multiple, source specific	Single
Reliance on non-satellite databases	Moderate	High

[1]Two-channel AVHRR data can be substituted for OLS data

3.2   DNA DATA SET DESCRIPTION

The DNA data requirements called for delivery of up to eight data sets collected over 10-day periods between September 1994 and March 1995 for four geographic locations (Figure 6). All available data for the 10-day periods from two DMSP, two NOAA/TIROS, and one geostationary satellite were analyzed through the SERCAA algorithms for each geographic location. Each data set consisted of SERCAA Level-1, Level-2 and Level-3 products for each of the 5 satellites plus hourly Level-4 integrated cloud analyses. The geographic regions were selected by DNA to be representative of the climatic and geographic conditions most stressing to the analysis and forecast models. In addition to the four ROIs identified in Figure 6, data from an earlier SERCAA study for three small regions over the Southeast Asian land mass and Western Pacific were included as an early demonstration set. Ultimately, funding limitations restricted the number of large-ROI data sets produced for DNA to four, two from EASA and one each from CNSA and EMDA. Summaries of data set attributes for the demonstration set plus the four ROI sets are provided in Tables 9 through 12.
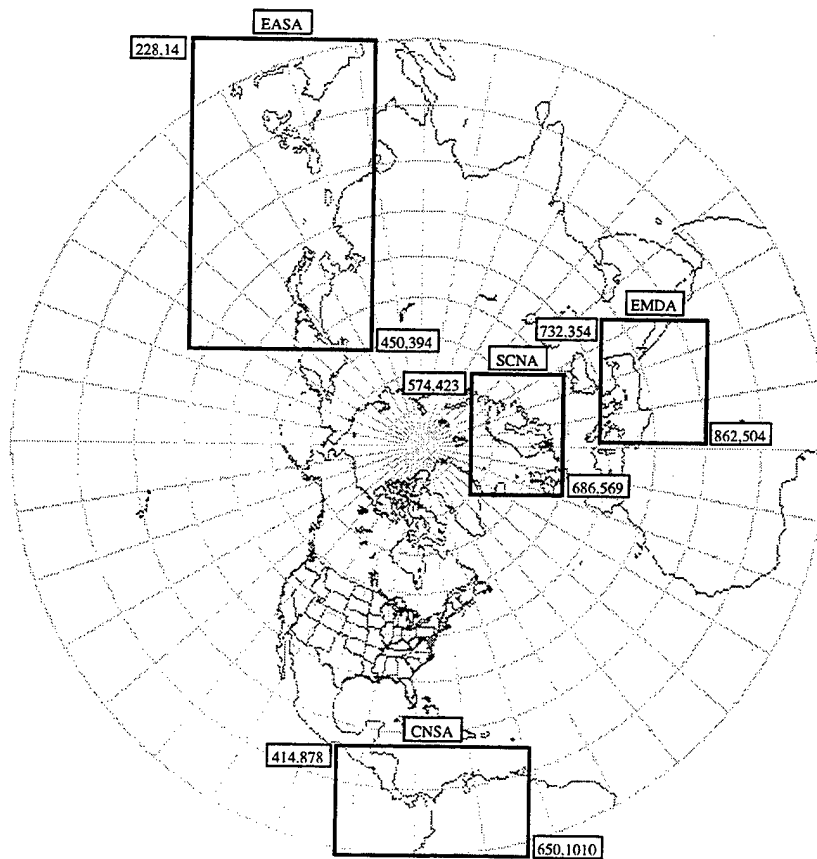
Figure 6 Regions of interest for DNA data study. Numbers associated with each ROI indicate 16th mesh grid box bounds.

Table 9 East Asia demonstration data set attributes

Data Set Description	Himalayas region	Japan region	Panama region
Region Name	HIM	JPN	PAN
Collection Period: Julian Dates	27-30 May 1993 93147 - 93150	27-30 May 1993 93147 - 93150	27-30 May 1993 93147 - 93150
Satellites	DMSP F10, F11 GMS-4 NOAA-11, 12	DMSP F10, F11 GMS-4 NOAA-11, 12	DMSP F10, F11 GOES-7 NOAA-11, 12
16th Mesh Grid (i,j)	(536,168) – (600,232)	(344,234) – (408,298)	(504,914) – (568,978)
i Range	$536 \leq i \leq 600$	$344 \leq i \leq 408$	$504 \leq i \leq 568$
j Range	$168 \leq j \leq 232$	$234 \leq j \leq 298$	$914 \leq j \leq 978$
Output Size	65 x 65 Grid Cells	65 x 65 Grid Cells	65 x 65 Grid Cells

Table 10 EASA satellite data set attributes

Data Set Description	Data Set Attributes	
Region Name	EASA-1	EASA-2
Collection Period: Julian Dates	22-30 March 1993 93081 - 93089	22-31 July 1993 93203 - 93212
Satellites	DMSP F10, F11 GMS-4 NOAA-11, 12	
16th Mesh Grid (i,j)	(227,13) – (451,395)	
i Range	$227 \leq i \leq 451$	
j Range	$13 \leq j \leq 395$	
Output Size	225 x 383 Grid Cells	

Table 11 EMDA satellite data set attributes

Data Set Description	Data Set Attributes
Region Name	EMDA
Collection Period: Julian Dates	12-21 March 1994 94071 - 94080
Satellites	DMSP F10, F11 METEOSAT-4 NOAA-11, 12
16th Mesh Grid (i,j)	(731,353) – (863,505)
i Range	$731 \leq i \leq 863$
j Range	$353 \leq j \leq 505$
Output Size	133 x 153 Grid Cells

Table 12 CNSA satellite data set attributes

Data Set Description	Data Set Attributes
Region Name	CNSA
Collection Period: Julian Dates	22-31 March 1994 94081 - 94090
Satellites	DMSP F10, F11 METEOSAT-3 NOAA-11, 12
16th Mesh Grid (i,j)	(413,877) – (651,1011)
i Range	$413 \leq i \leq 651$
j Range	$877 \leq j \leq 1011$
Output Size	239 x 135 Grid Cells

Sensor data from four polar orbiting environmental satellites (DMSP F10 and F11, NOAA 11 and 12) and four geostationary (METEOSAT 3 and 4, GOES 7, and GMS 3) were collected to support the DNA program. Each data set covers a 10-day period, normally the last ten days of a month. The various data sources used to obtain the required satellite sensor data for the selected time periods and ROIs are identified in Table 13. GOES 7 and METEOSAT 3/4 data were collected at the AIMS ground station facility, GMS data were obtained from the University of Hawaii, DMSP data were provided by the NOAA National Geophysical Data Center (NGDC), and NOAA/TIROS data by the NOAA National Climatic Data Center (NCDC). Data from each source were received in different formats and data quality varied widely. It was necessary to develop separate data ingest and quality assurance software for each data source. Ingest products included calibrated infrared brightness temperature and visible count data, Earth location information, and sun-satellite geometry information. All ingest data were maintained in the original satellite scan projection of the respective satellite systems.

Table 13 Satellite data sources

Satellite Platform	Data Source

DMSP
   F10
   F11
	National Geophysical Data Center (NGDC)
	Boulder, CO

GMS GMS-4	University of Hawaii
GOES GOES-7	AIMS Direct Readout Ground Station Phillips Laboratory Hanscom AFB, MA

METEOSAT
   METEOSAT-3
   METEOSAT-4
	AIMS Direct Readout Ground Station
	Phillips Laboratory
	Hanscom AFB, MA

NOAA
   NOAA-11
   NOAA-12
	National Climatic Data Center (NCDC)
	Ashville, NC

As previously discussed, the SERCAA cloud analysis algorithms use four levels of processing as summarized in Figure 5. Level 1 processing is data ingest. Tape data were processed through separate ingest programs for each data source and format. Modifications to the SERCAA software were required to support the specific DNA test site locations as well as new DMSP and GMS data formats. In addition, modifications to were needed to accommodate multiple orbits of NOAA/TIROS data. Data from each polar satellite orbit, or geostationary scan, that intersected one of the ROIs were ingested and stored on AIMS using SERCAA Database (SDB) management software developed earlier. All Level 1 data products for each orbit/scan were stored in a standard format with separate files maintained for each sensor channel plus two additional files containing Earth location and satellite/solar geometry information. Ingest products are described more completely in Section 2 of Gustafson et al. (1994).

Level 2 processing employs sensor specific nephanalysis algorithms for cloud detection. Level 1 sensor data from DMSP, NOAA, and the geostationary satellites are processed through the respective nephanalysis algorithms as following the procedure in Figure 5. One output file is generated for each orbit/scan and nephanalysis results are stored in original satellite scan projection.

Level 3 processing uses Level 1 and 2 products as input to stratify the cloudy regions into vertical cloud layers as well as to classify different cloud types. At this point in the processing chain output products are no longer provided at the individual pixel level, but represent statistical values accumulated over 16th mesh grid cells (see Hoke et al., 1981 for a description of the AFGWC polar stereographic map projection standard). Up to four cloud layers are identified for each grid cell. One Level 3 file was created for each set of Level 1 and 2 products associated with a single orbit/scan. All Level 1, 2, and 3 products associated with a single satellite pass are related through SDB and were provided to DNA on tape as a set.

Level 4 processing is a clock driven process with one new integrated analysis performed each hour. The integration algorithm operates on the most recent Level 3 gridded products available from each satellite source. As was the case with Level 3 products, the Level 4 output files conform to the AFGWC 16th mesh grid structure.

Software originally developed to support algorithm testing during the SERCAA program had to be extensively modified to handle the large volume of data required for the DNA

processing. The most extensive changes were required to the cloud layering and integration algorithms (Level 3 and 4 processing). During SERCAA these had been implemented at AER using the KHOROS rapid prototyping language. While well suited for algorithm development, KHOROS was too inefficient to accommodate the volume of DNA data. Thus, all Level 2 and 3 modules were rewritten from KHOROS to C using image processing software from the Image Processing Workbench (IPW). Also, since ingest and Level 2 processing were going to occur at the AIMS facility, it was necessary to port the code from AER to one of the SGI computers on AIMS to avoid a network bottleneck. This in turn required development of new automated communication software to handle database management between the SGI computers and preexisting VMS-based SDB software.

Hardware upgrades to AIMS were also required in order to improve the efficiency of the satellite data set production process. This hardware was required in order to accommodate the approximately 3 Gbytes of data products that comprise each data set. To achieve this, several key hardware items were specified by AER and purchased by the government for AIMS including two 8mm tape drives, two 1-Gbyte disk drives and 128 Mbytes of additional memory for the SGI computers.

3.3   ERROR CORRECTION

Feedback from users of the early DNA data sets identified several problems in the data that were determined to have been caused by program bugs that were subsequently corrected. These problems were: 1) a small percentage of clear pixels in the Level 3 analyses were incorrectly classified as missing and 2) data source information carried in the Level 4 audit trail contained valid entries for data that were no longer contributing to the integrated analysis because they had exceeded the age threshold.

Problems were encountered over the EMDA region with use of the available surface temperature climatology data that affected the accuracy of the Level 2 processing, particularly for METEOSAT data. The diurnal temperature trends observed in the climatological temperatures is out of phase with the clear-scene satellite measurements. There was an approximate six to nine hour shift in periods of peak cooling and heating between the clear-scene satellite measurements and surface temperature climatology that negatively impacted cloud analysis accuracy. This shift is depicted in Figure 7. To correct for this, a new reference background temperature database was developed for processing of METEOSAT data using the same technique developed for generation of visible clear-scene reference backgrounds. This

result provided good results over the desert background where the problem was most pronounced.
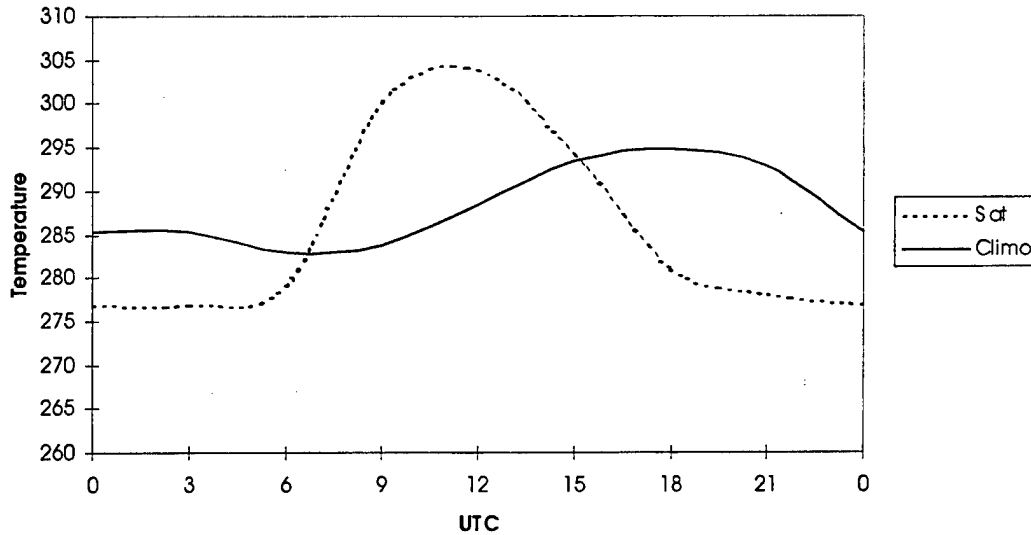

Figure 7 Diurnal temperature trends over the EMDA region

Periodic data dropouts and/or bad radiance values were found on numerous source data tapes that AER received for processing from NGDC. Considerable manual quality control efforts were required to identify and flag the most severely affected data files of which DMSP orbits were identified as the primary source. This effort was performed during Level 1 processing so that the most severely affected data files could be eliminated from further processing. Marginally affected orbits were allowed to pass through Level 1 processing with intermediate product and integrated analysis quality checks being performed again during Level 2 and 3 processing. If quality control checks determined that the intermediate product was of questionable quality then the entire orbit was removed from the satellite data set. Thus, any gaps in coverage on the delivered satellite data set tapes are due to either missing or bad data.

3.4 OUTPUT DATA SET ATTRIBUTES

A total of ten 8mm tapes were provided to DNA over the duration of the project. Table 14 provides a listing of these satellite data set tapes and their attributes. For data archiving purposes, all Level 1-3 products associated with a given satellite pass were placed in a single directory and subsequently stored on tape as a single tar file. Thus, the first tape for a collection period contains a series of several hundred tar files; each file contains all Level 1-3 products associated with a single satellite pass. Level 4 files are grouped on the second tape by day. This methodology was not followed for the two data set tapes for the EMDA region. Both of the

26

tapes for the EMDA region contain Level 1-4 products with the each tape covering different intervals of the collection period.

For each set of Level 1-3 products, and for each Level 4 file there is also an SDB Information File associated with it. These files contain descriptive metadata information extracted from the SERCAA Database that describe the relevant attributes of the SERCAA product files.

Table 14 Satellite data set tape attributes

Region Name	Collection Period	Table Label	Contents
EASA-1	22-30 March 1993 93081 - 93089	DNA MAR93 ENTRIES	Level 1-3 Products
		DNA MAR93 IA	Level 4 Products
HIM, JPN, PAN	27-30 May 1993 93147 - 93150	SERCAA RE MAY93 1	Level 1 & 2 Products
		SERCAA IA MAY93 1	Level 4 Products
EASA-2	22-31 July 1993 93203 - 93212	DNA JUL93 ENTRIES (RE)	Level 1-3 Products
		DNA JUL93 IA	Level 4 Products
EMDA	12-21 March 1994 94071 - 94080	DNA MAR94 EMD IA/RE 071-078	Level 1-4 Products for first 8 days
		DNA MAR94 EMD IA/RE 079-080	Level 1-4 Products for last 2 days
CNSA	22-31 March 1994 94081 - 94090	DNA MAR94 CNS ENTRIES (RE)	Level 1-3 Products
		DNA MAR94 CNS IA	Level 4 Products

4.0 SPACE-BASED INFRARED SYSTEM (SBIRS)

The SBIRS Phenomenology Exploitation Project (PEP) was tasked with investigating the impact of cloud on proposed systems. In support of that project, two tasks were identified under the contract: 1) evaluate of alternative approaches for retrieval of cloud height, optical depth, and emissivity from environmental satellite data and select an optimal approach that builds on the SERCAA algorithms; 2) use the selected algorithm to compute analyzed cloud products for specific regions and times coinciding with observations made by PEP-directed aircraft, ground based, and satellite observing systems; and 3) compare results from the selected algorithms to coincident results from the CO_2 slicing model.

4.1 MEASUREMENT OF CIRRUS PROPERTIES

Many sources of passive satellite data are potentially useful for detection and analysis of cirrus attributes. Among the earliest are visible and infrared data of the 1960s from the TIROS series of polar orbiting satellites, augmented in the early 1970s by geostationary GOES data. Current GOES Atmospheric Sounder channels useful for detection of cirrus include 3.9, 6.7, 11.2, 12.7, and CO_2 13.3 - 14.5 μm spectral bands. The 3.9 and 11.2 - 12.7 μm channels will be discussed in detail shortly; the 6.7 μm water vapor band has proven useful for detection of very thin cirrus over warm backgrounds such as deserts and tropical oceans.

More recent TIROS satellites have include the Advanced Very High Resolution Radiometer (AVHRR), a five-channel passive radiometer with detectors that measure upwelling visible (0.63 μm), near-infrared (NIR, 0.86 μm), middle wavelength IR (MWIR, 3.7 μm), and split longwave IR (LWIR, 10.7 and 11.8 μm) energy both day and night. The sounder instruments collectively known as TOVS (TIROS Operational Vertical Sounder) also collect data in the wings of the 15 μm CO_2 absorption band that are useful for detection of thin cirrus and specification of their height. There are also very high spatial resolution (500 m) Defense Meteorological Satellite Program data available in visible/NIR (0.4 - 1.1 μm) and LWIR (10 - 12 μm) bands that are helpful in ascertaining the small-scale spatial attributes of cirrus.

Cirrus is recognized as one of the most poorly quantified of all clouds. Cloud altitude is difficult to specify, because cirrus typically consist of ice particles distributed over a considerable vertical extent with complex optical properties and microphysics. In addition to the wide variability in properties common for other cloud types, cirrus clouds are unique in

28

exhibiting a range of transmissivity values τ that span the entire possible domain $0 < \tau < 1$. Transmissive cirrus clouds both emit and transmit thermal energy. Emissions occur at a rate dependent on cirrus emissivity and temperature, while transmissions depend most strongly on cirrus transmissivity and the temperature of the underlying warmer surface (either a lower cloud or the ground). Physical retrievals of cirrus radiative and spatial properties must account appropriately for these attributes. If the semi-transparent nature of cirrus clouds is not properly modeled, its altitude is consistently underestimated when using passive infrared brightness temperature data.

Other uncertainties in satellite-retrieved cirrus attributes include thin cirrus fraction altitude, and thickness because the measured cirrus signal is affected by both cloud and the surface below. A more accurate determination of cirrus attributes is needed on both global and local spatial scales. Schiffer and Rossow (1983) specify the ISCCP goal of 30-day average cloud fraction to an accuracy of +30% for global total cloud; required cirrus accuracy is re specified to be ±5% for fraction, and ±1 km for altitude.

The transmissive nature of cirrus cloud turns out to be its most important (in a climate sense) and elusive (in a retrieval sense) attribute to specify. If the semi-transparent nature of cirrus is not accounted for, its altitude is consistently underestimated when using passive infrared brightness temperature data. Although it is generally agreed that cirrus has a net warming effect on climate, determination of the magnitude of this effect depends critically on the accurate specification of cirrus radiative and spatial attributes. For example, in the case of very thin ("sub-visual") cirrus, ice particles have a more significant interaction effect with incident solar and upwelling thermal radiation than does upper tropospheric water vapor (Smith et al., 1990).

Early cirrus climatologies (1979 - 1981) include those obtained using SAGE limb sounder data (Woodbury and McCormick, 1983). A solar disc extinction analysis technique was used to determine the presence of high-altitude cirrus at a spatial resolution of 100 km^2. In the early 1970s, a limited amount of Nimbus-4 IRIS infrared data were analyzed to detect the presence of cirrus over ocean between ±50° latitude (Barton, 1983). The most extensive cirrus climatologies to date are those compiled at the University of Wisconsin since the mid-1980s using the CO_2 slicing technique. CO_2 slicing is used with NOAA geostationary and polar orbiting satellite sounder channel data to retrieve cirrus altitude and effective emissivity (Wylie and Menzel, 1989).

The CO_2 technique estimates cirrus altitude and the product of cloud fraction (N) and emissivity (ϵ), called effective emissivity (Nϵ). This technique uses satellite-measured radiance from the NOAA High-Resolution Infrared Radiation Sounder (HIRS) and GOES-sounder CO_2 channels in the 13.4 - 14.2 μm spectral range. It is capable of detecting the presence of transmissive cirrus clouds at levels in the upper troposphere above where the CO_2-channel weighting functions peak. The differential absorption characteristics within the sensor spectral bands allows the CO_2 slicing method to detect transmissive cirrus and specify their height. Once the presence and effective altitude of transmissive cloud is established, an IR window-channel brightness temperature measurement is used along with an estimate of the surface skin temperature to compute effective emissivity. If the CO_2 channel radiance fail to reliably detect the presence of transmissive cloud, an emissivity of 1.00 is assumed and IR temperature is compared to a temperature profile to assign a blackbody, opaque cloud top altitude. A detailed description of the CO_2 slicing technique is given by Wylie and Menzel (1989).

4.2   CIRRUS RETRIEVAL ALGORITHM

SERCAA cloud algorithms are described in Section 3.1. Modifications were made to the SERCAA Phase I geostationary algorithm to exploit the additional full-time GOES-8 imager channels (3.9 μm and split LWIR). Due to the similar channel characteristics between GOES-8 and AVHRR, these modifications were primarily a programming effort. Testing was performed to verify that the changes made to the algorithm provided the results that were expected based on results of the already established and tested SERCAA Phase I AVHRR algorithms. SERCAA Phase I algorithms, for all platforms, were also modified to produce fewer number of cloud layers with greater temporal consistency as compared to SERCAA Phase I results. This modification was made in accordance with feed-back from DNA.

In addition to cloud detection, advances made during SERCAA Phase II were added to the Phase I software to retrieve altitude information, effective emissivity and optical depth statistics for cirrus from AVHRR and GOES-8 data. Initial versions of these algorithms only operated on nighttime data due to contamination of 3.7 μm measurements by reflected solar during the daytime. However, experiments splitting out the reflected and emitted components of the measurements, coupled with use of 6.7 μm channels, have shown good results during daytime conditions.

4.2.1 PASSIVE INFRARED PHYSICS OF CIRRUS CLOUD SIGNATURES

The upwelling spectral thermal radiance I_{obs} measured by a downward pointing radiometer for a field-of-view completely filled by a non-reflective, thin cirrus cloud is:

$$I_{obs} = (1-\varepsilon) \, I_{sfc} + I_{cld},\qquad(1)$$

where ε is the bulk cirrus emissivity, I_{sfc} is the upwelling radiance emitted by the underlying surface and clear atmosphere, and I_{cld} includes the cirrus blackbody radiance plus the radiance emitted by the atmosphere above the cloud. In practice, the non-reflective nature of cirrus clouds at thermal infrared wavelengths allows us to neglect reflectance. This is a reasonable assumption not only because the cirrus bulk reflectivity is low, but also because there is only minor down welling thermal emission incident on the top of cirrus clouds to be reflected back to space.

In theory, specification of I_{sfc}, in Eq. (1) requires information on many of the physical properties of the atmosphere and surface that underlies the cirrus cloud: the temperature T_{sfc} and atmospheric transmittance τ (for water vapor attenuation) are two of the more important attributes. As discussed later, I_{sfc} is specified using nearby measurements of cirrus-free pixels.

The two unknowns of interest in Eq. (1) are the cirrus bulk emissivity ε and the cirrus Planck blackbody emission I_{sfc} which is a known function of the cirrus effective temperature T_{cld} In contrast, there is only one known in Eq. (1), namely the radiance I_{obs} in order to specify these two unknowns, additional measurement information is needed. This is achieved first by considering Eq. (1) for simultaneous radiance measurements at two different infrared wavelengths.

For purposes of discussion, assume that the radiance data are being measured by the AVHRR MWIR Channel 3 and LWIR Channel 4 sensors. The two cirrus radiance equations are then:

$$I_{obs,3} = (1 - \varepsilon_3) \, I_{sfc,3} + \varepsilon_3 \, I_{cld,3}\qquad(2a)$$

and

$$I_{obs,4} = (1 - \varepsilon_4) \, I_{sfc,4} + \varepsilon_4 \, I_{cld,4}\qquad(2b)$$

where the "3" and "4" subscripts denote the 3.7 and 10.7 μm AVHRR Channels 3 and 4 radiance, respectively. Eqs. (2a) and (2b) are two equations, but with the second equation a third unknown ε_4 has been introduced.

A third equation is needed that contains no new variables and that relates at least two of the three unknowns already established. This is done by assuming a relationship between the cirrus bulk optical depths δ_3 and δ_4 as follows. First, radiative transfer calculations are available that compute bulk cirrus optical depth as a function of wavelength and hexagonal ice particle size for varying cirrus cloud thickness (Takano and Liou, 1989; Hunt, 1973). Once computed, a simple linear regression between corresponding pairs of the two optical depths is performed to obtain a relationship of the form

$$\delta_3 = m\,\delta_4 + b, \tag{3}$$

where m and b are the regression slope and intercept, respectively. The slope m is nonzero; the intercept b, however, turns out to be very close to zero since the optical depths measured at the two wavelengths are close to each other for optically very thin cirrus. Thus, Eq. (3) is generally of the form

$$\delta_3 = m\,\delta_4. \tag{4}$$

The slope m turns out to be well parameterized by ice crystal size, which in turn is strongly associated with cirrus environmental temperature. Ou et al. (1993) parameterize ice crystal size as

$$L = c_0 + c_1\,(T_{cld}\text{-}273) + c_2\,(T_{cld}\text{-}273)^2 + c_3\,(T_{cld}\text{-}273)^3 \tag{5}$$

where L is the effective ice crystal size (μm); $\{\,c_0, c_1, c_2, c_3\,\} = \{326.3, 12.42, 0.197, 0.0012\,\}$; and where T_{cld} is the cirrus effective temperature (K). The slope m is then given by:

$$m = a_0 + a_1/\,L + a_2\,/\,L^2, \tag{6}$$

where $\{\,a_0, a_1, a_2\,\} = \{\,0.722, 55.08, -174.12\,\}$ (after Ou et al., 1993). Figure 8 contains a plot of the regression slope m as a function of cirrus effective temperatures T_{cld} between 210 K and 253 K.
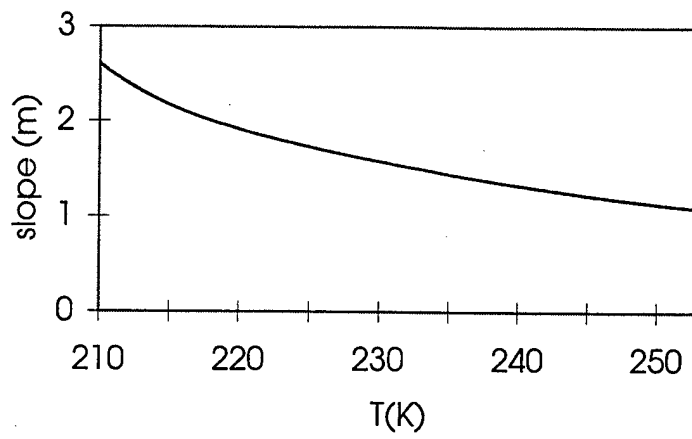
Figure 8 Plot of m in Eq. 6 as a function of temperature

Considering the radiative properties of cirrus within a satellite field-of-view in a bulk sense, the cirrus cloud optical depth δ is related to the cirrus transmissivity τ by the relation

$$\delta = -\ln \tau \qquad (7a)$$

so that Eq. (4) can be written

$$\ln \tau_3 = m \ln \tau_4. \qquad (7b)$$

Since it is assumed that the cirrus cloud in non-reflective, $\varepsilon + \tau = 1$ so that

$$\ln (1-\varepsilon_3) = m \ln (1 - \varepsilon_4). \qquad (7c)$$

Finally, solving for ε_3 in terms of ε_4 yields

$$\varepsilon_3 = 1 - (1 - \varepsilon_4)^m. \qquad (8)$$

This is the third of the three-set equation, so that there are now three equations (2a), (2b), and (8) in three unknown ε_3, ε_4, and T_{cld}. The three measurements consist of the linear regression slope m, and the satellite-measured radiance $I_{obs,3}$ and $I_{obs,4}$. This three-equation system forms the basis for most cirrus retrieval techniques that analyze multispectral infrared satellite radiance.

In practice, nearby cirrus-free pixels are used to obtain accurate estimates of $I_{sfc,3}$ and $I_{sfc,4}$. Atmospheric emission above the cirrus is neglected. Also assumed in Eqs. (2a) and (2b) is that any reflection from the cirrus cloud can be neglected. At LWIR wavelengths this assumption is reasonable since both the cirrus bulk reflectivity is low and there is only minor downwelling thermal energy incident on the top of cirrus clouds to be reflected back to space. However, for the LWIR data, reflection of incident solar energy during daytime cannot be considered negligible and the validity of Eq. (2a) becomes suspect. If the series of Eqs. (2a), (2b), and (8)

33

do not provide an accurate description of the radiant energy balance then the cirrus retrieval process becomes considerably more complex. Ou et al. (1993) have developed a technique to separate out the solar component in the 3.7 μm daytime data that is potentially applicable to this problem.

Pursued in light of the 3.7-μm daytime solar contamination issue, ongoing studies are revealing that 6.7-μm water-vapor channel data can be used for the MWIR-channel data in place of those taken at 3.7-3.9 μm data used above in the cirrus retrieval algorithm. This finding is significant in that (a) the complexity of retrieving cirrus properties during daytime (due to mixed solar/thermal energy at 3.7- μm) is eliminated, and (b) there are 6.7-μm water vapor channels on all currently operational meteorological satellites, both geostationary and polar, save DMSP. Thus, with the development of a 6.7 μm cirrus optical depth and effective altitude algorithm comes a capability for cirrus spatial and optical property analyses that are truly global in nature and that span the full diurnal cycle. The water-vapor cirrus retrieval physics is identical to the MWIR retrieval physics so that Eq. (2a) is rewritten to use 6.7 μm in place of 3.7 μm satellite radiance observations, and Eqs. (5) and (6) are replaced by

$$m = 1. \tag{9}$$

The underlying premise is that cirrus optical properties are very similar between 6.7 and 10.7 μm (Kuo-Nan Liou, personal communication).

Another major constraint of this cirrus retrieval approach is that in assigning a single cloud temperature T_{cld} to the cirrus, it is assumed that the cloud is a thin sheet that lies precisely at one atmospheric level. Clearly this is not the case. Lidar backscatter returns from cirrus clouds consistently show their complex structure on both horizontal and vertical scales. In mid-latitudes their altitudes range from 6 to 13 km, and their thickness anywhere from 1 to 5 km and, on occasion, even higher. Thus, the assignment of a single cirrus temperature is a gross one which in the case of multispectral infrared radiance retrievals results in the assignment of one effective cirrus cloud altitude. However, the severity of this constraint affects only the cirrus altitude determination. Its effects on the bulk optical properties of the cloud are far less detrimental. Nonetheless, it is important to remember that current satellite-retrieved cirrus altitudes are not an accurate assessment of the true levels at which the cirrus lie, but rather are only correct in a radiatively bulk, energy-average sense. For this reason the cirrus temperature T_{cld} and

corresponding altitude z_{cld} are labeled as "effective" properties, since they afford little inference on the detailed vertical structure of the cloud.

In practice Eqs. (2) and (8) can also be used with AVHRR channels 3 and 5. Thus, for every triplet of AVHRR infrared satellite radiance measurements $I_{obs,3}$, $I_{obs,4}$, and $I_{obs,5}$ it is possible to retrieve at sensor resolution the 3.7, 10.7, and 11.8 μm cirrus bulk emissivities ε_3, ε_4, ε_5 and optical depths δ_3, δ_4, δ_5, along with cirrus effective temperature (altitude) T_{cld} (Z_{cld})

4.2.2 MULTISPECTRAL INFRARED CIRRUS BRIGHTNESS TEMPERATURE DIFFERENCES

There are three main reasons why cirrus detection using multispectral infrared measurements is successful at night. The most dominant effect has to do with the nature of the dependence of the Planck function on temperature at the three AVHRR IR wavelengths. To illustrate this, consider the simple example in which a pixel contains a cirrus cloud of temperature 230 K and emissivity 0.5, and under which lies a background surface of 280 K. (For now, ignore atmospheric effects and the fact that the cirrus emissivities are not constant from one channel to the next. These issues are discussed later.) According to Eq. (1), in this situation half of the measured upwelling radiance in each channel will originate from the cold cloud at 230 K and the other half from the underlying warm surface at 280 K. Using the Planck function, the proportions of the total radiance (half cloud and half background) that are measured by the satellite can be computed; results are plotted in Fig. 9. Note that proportionally less energy comes from the warmer part of the scene as wavelength increases; this effect is due solely to the exponential dependence of the Planck function on temperature at the three wavelengths. The resulting brightness temperatures are also plotted in Figure 9; note the high, positive differences $T_3 - T_4 = 8.4$ K $(\Delta T_{3,4})$ and $T_3 - T_5 = 8.9$ K $(\Delta T_{3,5})$. Such brightness temperature differences are consistently and distinctively characteristic of thin cirrus clouds in nighttime AVHRR data.
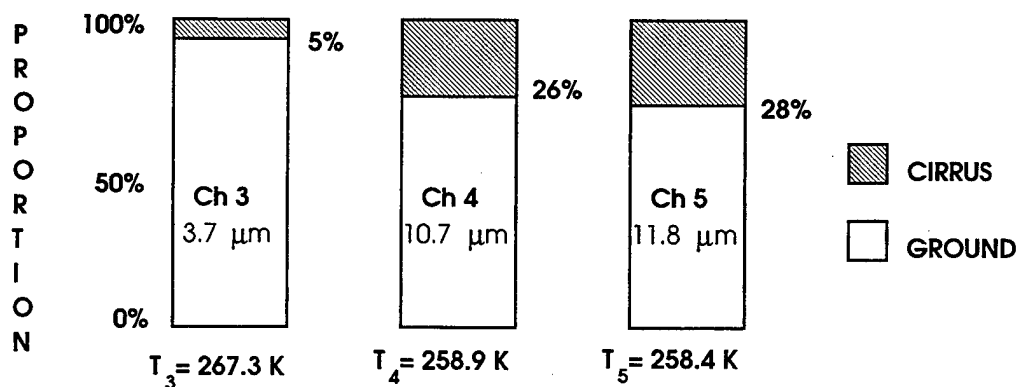

Figure 9 Cirrus brightness temperature difference at AVHRR channels 3, 4, and 5

The second effect is that of the varying emissivities of ice particle clouds themselves among the three wavelengths. In general, cirrus emissivities increase with increasing wavelength for the three AVHRR infrared channels. This means that, on the basis of emissivity alone, increasingly more of the upwelling radiant energy in a cirrus filled pixel comes from the colder cloud. This is an complementary but weaker effect to that of the Planck function in that it amplifies the brightness temperature differences which comprise the thin cirrus signature.

Finally, the third effect that causes brightness temperatures for cirrus pixels to decrease with increasing wavelength is that of varying atmospheric water vapor attenuation. In general, atmospheric water vapor attenuation is stronger at longer wavelengths. This operates in the same sense as do the previous two, increasing the difference between channel 3 and channels 4 or 5 brightness temperatures, although typically it is the weakest effect of the three.

T_4-T_5 differences for ice particle clouds are also due to the same reasons; however, the dominant effect in this case is that of changing emissivity. This is mostly due to that fact that channels 4 and 5 are spectrally too close to one another for the Planck temperature dependence differences to manifest themselves as significantly as they do for 3.7 μm. However, even though the differences tend to be smaller, they are very consistent for thin cirrus, especially very thin cirrus.

In summary, the cirrus property retrieval algorithm described above exploits: 1) the stronger dependence of the Planck function on temperature at 3.7 μm wavelengths; 2) the differences in emissivities at each of the three AVHRR IR wavelengths as described by Eq. (8); and 3) stronger atmospheric water vapor attenuation in the longer wavelength regions (i.e., 10.7 and 11.8 μm). Interchannel temperature differences are highest for cirrus clouds with bulk emissivities of approximately 0.8 to 0.9, and with higher effective cloud altitudes of 10 to 13 km.

4.2.3 TESTS AND RESULTS

Nighttime AVHRR data for Channels 3, 4, and 5 were obtained over New England at ~2337 UTC on 16 September 1995, a time when surface-based radar observations of thin cirrus were available at Hanscom AFB as a part of ongoing SBIRS field observations. The Hanscom site was equipped with a TPQ-11 ground-based active radar system. The TPQ-11 is a 35GHz upward-pointing radar that provides useful observations of cirrus cloud base and top against which satellite retrievals can be directly compared. AVHRR High-Resolution Picture Transmission (HRPT) data were used. Each HRPT pixel has a resolution of approximately 1

km at nadir. The AVHRR image sample over Hanscom is close to satellite nadir, and was selected for the following reasons: 1) there were abundant thin cirrus in the southern New England area; 2) atmospheric sounding information from nearby RAOB stations was readily available, valid for the time and location of the thin cirrus observations; and 3) surface-based lidar observations of the cirrus were collected for a period before, during, and after the NOAA satellite overpass time. The radar observations serve as a best source of ground truth for verifications of calculated Z_{cld}.

Subsequent satellite retrieval results are then compared to the cirrus radar observations to help verify (or at least substantiate) the calculations of Z_{cld}. It is not possible to verify the cirrus emissivity estimates except to say that if the effective cirrus altitudes Z_{cld} are reasonable, then the emissivities are also likely to be reasonable since these two parameters are coupled in the physical retrieval model.

The emissivity and effective altitude estimates obtained for the Hanscom cirrus sample using the enhanced cirrus algorithm to analyze AVHRR infrared Channels 3 and 4 data are plotted in Figure 12. Pixel-by-pixel measurements of brightness temperature pairs T_3 and T_4 were selected ±30 minutes upwind and downwind of the radar site within the cirrus clouds. The model-generated cloud altitudes for these pixels are consistent with TPQ-11 ground-based radar measurements of cirrus cloud base and top. The TPQ-11 radar measured cirrus base and tops in the 5.5 - 10 km range for the time period several hours before and after the 2337 UTC satellite overpass. The retrieved cirrus effective altitudes agree well with the radar observations of cloud
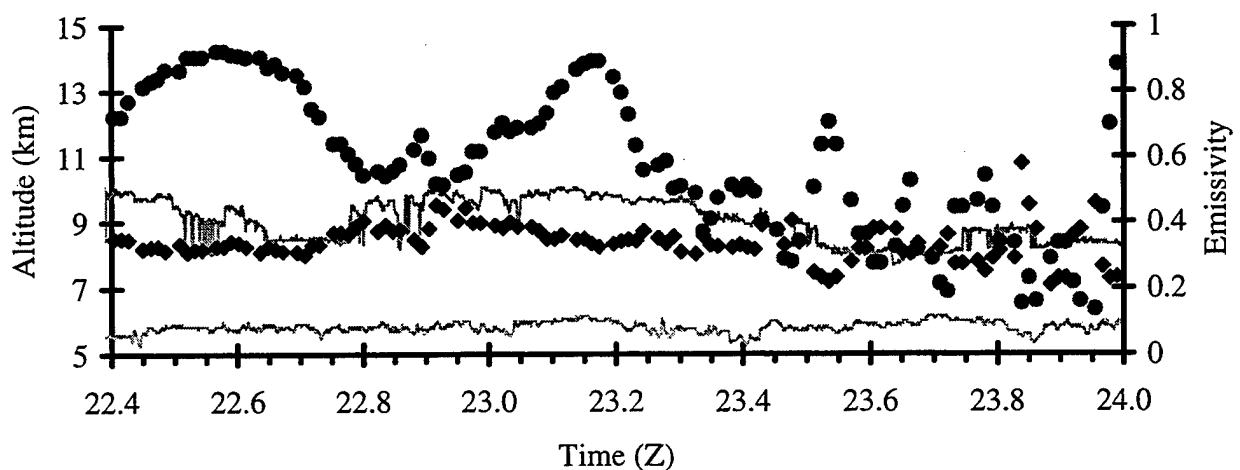

Figure 10 Enhanced cirrus cloud-top (diamonds) and emissivity (circles) retrievals over Hanscom AFB compared to TPQ-11-derived cloud top and base (solid lines)

37

base and top, lending confidence that the transmissive characteristics of the thinner cirrus are being properly accounted for in the model.

Altitude retrievals that do not take into account the transmissive nature of cirrus, so called "blackbody" cirrus altitudes, were also generated and compared to the radar-generated heights. Blackbody altitudes are obtained by simply 1) comparing the Channel 4 thin cirrus brightness temperature directly to the atmospheric temperature profile, and 2) choosing that height whose temperature matches the observed brightness temperature. In Figure 11 are plotted the blackbody altitudes along with the cirrus algorithm retrievals. Differences between the two retrievals are small where effective cirrus emissivity is close to one (the left side of the plot), on the order of a few hundred meters. However, differences between the two retrieved altitudes increase substantially as the cirrus becomes more optically thin (right side of plot). For the very thinnest of clouds this difference in altitudes is on the order of 5 km, as can be seen in Figures 10 and 11. These results quantitatively illustrate the importance of accounting for transmissive cirrus effects when trying to retrieve accurate cirrus altitudes from satellite.
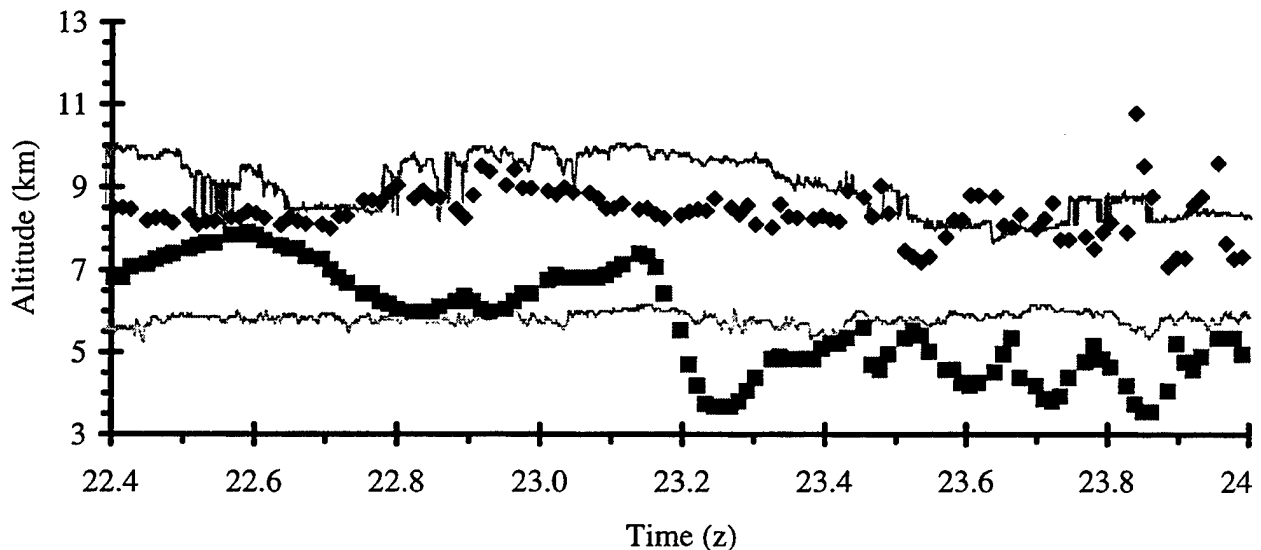
Figure 11 Enhanced cirrus retrievals (diamonds) over Hanscom AFB compared to TPQ-11-derived cloud top and base (solid lines) and blackbody retrievals (squares)

Although the size of the sample set is small, these comparison results demonstrate that it is feasible to accurately compute effective altitude and cirrus emissivity, transmissivity, and optical depth at multiple wavelengths on a pixel-by-pixel basis using the principles and techniques described above.

4.3   SBIRS ANALYZED DATA SETS

As identified above, the objective of the second SBIRS task was to use the selected cirrus retrieval algorithm to compute analyzed cloud products for specific regions and times coinciding with observations made by PEP-directed aircraft, ground based, and satellite observing systems. Two large data sets were analyzed through the enhanced cirrus algorithms for the SBIRS program. The first set consisted of two months of high resolution AVHRR and GOES data analyzed over the central and eastern U. S. and the western Atlantic (Figure 12). The AIMS NOAA and GOES satellite ground stations were used to acquire all AVHRR data over the region of interest from NOAA 12 and 14 and three-hourly GOES-8 data (0,3,6,9,12,15,18,21 UTC) during the months of August and September 1995. The second data set included GOES and NOAA data from September 1996 over Florida and the south east U.S (Figure 12). Occasional data gaps exist in the GOES data at this time of year due to the normal Equinox eclipse periods during which the satellite passes into the Earth shadow requiring observations to be suspended for a few hours each day to conserve electricity. Basic cloud-detection processing was performed using the SERCAA Phase 1 and 2 algorithms described by Gustafson et al. (1994). Further processing then occurred using the cloud phase and cirrus altitude retrieval algorithms described in Section 4.2 above. The final products are pixel-level representations of cloud amount as a function of optical-property-retrieval-corrected altitude, pressure, and emissivity. Additional data includes latitude and longitude for each pixel.
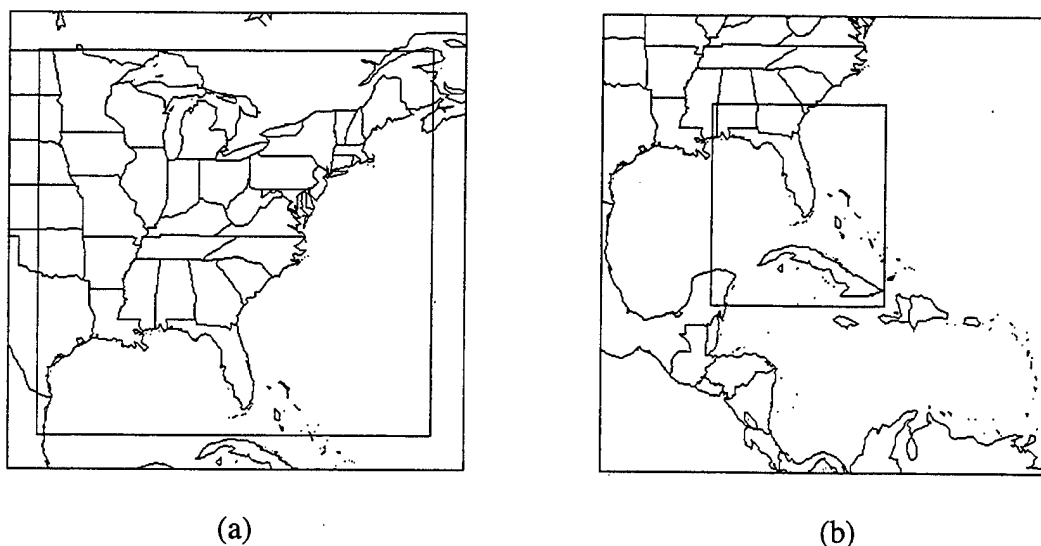

(a)   (b)

Figure 12 SBIRS data collection and analysis areas for 1995 (a) and 1996 (b)

For the 1995 data set, analyzed output frequency was every 3 hours on a pixel-by-pixel basis for the full two-months of the observation period. During that time period, SBIRS ran several instrumented aircraft missions in the analysis region and numerous ground-based radar and lidar measurements were made at Hanscom AFB, MA and Madison, WI, respectively. The required cloud parameters computed are layer cloud location, effective altitude, and emissivity. This task required the collection of NOAA/AVHRR HRPT and GOES-8 GVAR imager data. Since all satellite data collection was performed using the AIMS GOES and NOAA/POES ground stations, selection of the study areas was necessarily constrained both by SBIRS requirements and by the line of site requirement for AIMS NOAA polar-orbiting data (Figure 12a) and the data archive capabilities for the GOES data.

The 1996 data set, analyzed over Florida, was in coordination with over flights of two satellites known as the Midcourse Space Experiment (MSX) and the Miniature Seeker Technology Integration (MSTI). These, along with a high-altitude aircraft known as ARES, made a series of measurements over various locations around the globe, including the Florida site, during 1996. The corresponding environmental satellite data were collected and provided by AER for cloud analysis processing. Polar-orbiting data were collected from the orbits intersecting the region of interest that occurred immediately before and after the mission time. Differences of up to four hours between the mission time and the time of both polar passes were accepted. Geostationary data were collected for the two closest time periods occurring before and after the mission time plus the time period immediately preceding the first time period (SERCAA geostationary algorithms require data from at least two consecutive observations separated in time by a minimum of one hour).

Evaluation of the SERCAA Phase I (Gustafson et. al., 1994) AVHRR and Geostationary algorithms as well as the enhanced SERCAA Phase II (d'Entremont et. al., 1996) AVHRR and GOES-8 algorithms was performed in conjunction with analysis of the satellite data collected during the two study periods. Similar to the pilot study described in Section 4.2.3 above, reference cloud base and top altitudes were derived from near-coincident ground-based TPQ-11 radar located at Hanscom AFB and lidar measurements collected at the University of Wisconsin, located in Madison, WI. The radar and lidar measurements were made in coordination with SBIRS aircraft missions. Cloud altitudes were defined by applying thresholds to these radar and lidar data. Comparisons were then made between the satellite/lidar-derived values using both versions of SERCAA algorithms to the reference radar/lidar altitudes. Radar/lidar time-series

40

measurements were compared to areal satellite-retrieved values by converting from (radar/lidar) time coordinates to (satellite) spatial coordinates using a trajectory field based on cirrus-altitude winds over radar/lidar site. Comparisons are performed out to ±30 minutes from valid time of the satellite overpass. Comparisons were generally done graphically but standard comparison statistics (e.g., mean, standard deviation) were also generated for a few cases.

4.3.1 DATA PROCESSING

The SBIRS Optical Property retrieval program described above was used to assign cloud location, altitude, and emissivity for each scene. Processing was performed on a per pixel basis using a cloud mask generated by the SERCAA cloud analysis program. The same program was used on both the NOAA and GOES data. Output products were generated as a series of 8-bit TIF files, each at the same resolution as the input satellite data. Altitude, and emissivity at 3.7, 6.7, and 10.0 μm and geo-location data were produced. Retrievals were evaluated for meteorological validity and spatial uniformity. Approximately 100 images were inspected to assure consistency of results.

Processing consisted of five modules: satellite data ingest, clear colum temperature calculations, upper air retrieval, an implementation of the cirrus emissivity/altitude algorithm and product generation.

1) **Satellite Data Ingest:** Satellite data required for the cirrus emissivity/altitude algorithm are 3.9, 10.5 and 11.5 μm channel imagery from AVHRR and 6.7, 10.5, and 11.5 μm data from GOES. All sensor data were archived using the AIMS SERCAA Database (SDB). In SDB, images from a satellite pass are stored as scaled 8-bit pixels at a fixed resolution for each satellite system, for AVHRR this is 1 km, for GOES it is 4 km. The data ingest module calibrates and Earth locates the satellite telemetry data and produces the database records.

2) **Clear Column Temperature Calculation:** cloud property retrievals are based on the deviation of the observed temperatures from reference clear column temperatures, therefore the calculations are highly sensitive to both the absolute value and the variation of clear column temperature within a scene. Competing requirements of accuracy in retrieved properties and "smoothness" of expected results led us to evaluate a variety of strategies for determining clear column temperatures.

Climatology data derived from the AFGWC SFCTMP model were evaluated as a source for clear column temperatures. This provided smooth results at the expense of accuracy. A conscious goal was to minimize reliance on climatology and utilize contemporaneous satellite imagery data.

Initially, we assumed that the nearest cloud-free (CLEAR) pixels would provide the most accurate surface temperature estimate. For each cloudy pixel, we searched the scene to find the n closest pixels identified as CLEAR in the cloud mask, where n was allowed to vary from 3-50 pixels. The resulting altitude assignment was "blocky" (i.e., piecewise continuous) and varied with the search distance required to locate the CLEAR pixels. We constrained the search to 200 km radius and imposed a low limit (7) on the number of pixels averaged. Climatology was used for pixels where no nearby clear data could be found. This improved the results, although discontinuities were still observed and run times were excessively long (e.g., >100 min. for 500 X 1500 pixels).

With such large search neighborhoods, we decided that accuracy would not be sacrificed if we used the same clear column temperatures for all pixels within a neighborhood. Separate values for geography types (land/water) were maintained since combined types removed natural variation and distorted the altitude results. Clear-scene temperature calculations occur only twice per neighborhood, once each for land and water backgrounds. Processing performance improved by more than an order of magnitude with no noticeable loss of accuracy.

For large cloud masses, discontinuities in retrieved cloud altitude were introduced when the clear scene temperatures were chosen from different sides of a cloud mass. These artificial discontinuities were removed by providing for overlap of the neighborhoods. Our results showed that substantial overlap on large neighborhoods represented the best approach. In each neighborhood, clear scene temperatures were taken as the average temperature, after eliminating the coldest 5% and warmest 10% of pixels. Separate temperatures were stored for land and water points. Coastal boundary locations were treated as land.

The final processing algorithm works by first dividing the scene into neighborhoods of approximately 700 km^2 for calculation of clear scene temperatures. Results showed that

a substantial overlap of approximately 40% of these large neighborhoods produced the most consistent analysis.

3) **Upper Air Data:** Upper air temperature and moisture profiles were used by the SBIRS optical property retrieval program to convert cloud-top temperature information to cloud altitude and pressure. Gridded LFM analysis fields obtained from NCAR/UCAR for August and September, 1995 were used to provide the required upper air data between 20-50N and 50-100W. Available LFM fields included geopotential height (up to 500 mb), temperature for all available levels (up to 200 mb), dew point temperature (up to 300 mb) and surface temperature.

Twice-daily radiosonde observations were used to augment the LFM fields at upper levels. A latitudinal climatology of temperature, dew point temperature and height was calculated for mandatory pressure levels between 1000 and 200 mb using radiosondes located within the eastern US and Canada. To be used, the sounding had to go up to at least 500 mb and reported pressure interval below 500 mb must be less than 150 mb.

LFM and radiosonde-derived data were combined so that each LFM grid cell contains geopotential height, air temperature, and dew point temperature for 15 levels (i.e., 1000, 950, 900, 850, 800, 750, 700, 650, 600, 550, 500, 450, 400, 300, 250, 200 mb). Radiosonde data were interpolated to the intermediate levels. Any biases between the LFM data and radiosonde data were removed from the radiosonde data at the interface level to produce a smooth continuous profile. The resulting profiles were analyzed for discontinuities and none were found.

4) **Cirrus Emissivity/Altitude:** cirrus emissivity and altitude retrieval algorithms described above in Section 2 were implemented on AIMS and used to analyze the AVHRR and GOES data collected during the two-month period. Sensor data were first analyzed through the SERCAA cloud detection algorithms to discriminate clear and cloudy pixels. Cloud pixels were further segregated into two categories: transmissive cirrus and all others.

5) **Product Generation:** products were generated on a per pixel basis. Images for altitude, pressure and emissivity are 256 gray shade, 8-bit LZW compressed TIF files. They are viewable using a variety of public domain viewers that support TIF format (e.g., xv,

Khoros, IPW) as well as internally developed satellite image viewers available on AIMS. For each analyzed scene there is a TIF file for retrieved location, altitude, pressure, and emissivity at 3.7 or 6.7 and 10.5 μm. The data are in the original satellite projection and resolution. Latitude and longitude are stored as C language short integer, using the positive North, East convention. Values given are degrees*10 (e.g., 2935 = 293.5 K). Altitude values are scaled in increments of 1/17 km (i.e., 0-255 is Linear 0-15 km). Pressure values are mb/10 (e.g., 63 = 630 mb). Emissivity values are ε*100 (e.g., 21 = .21). Altitude values 1 and 254 are reserved for missing data.

4.3.2 DATA QUALITY

Results of the cirrus-property retrieval were validated manually by visualizing synthetic images of the product fields and through comparisons to ground-based lidar and radar measurements. Two problems remain and cause some altitude fields to contain a few anomalous values (manifested as speckles in a synthetic image). We were able to identify two sets of conditions external to the algorithms which led to these anomalous values.

In one set of cases, pixels on the edges of cloud masses were assigned unreasonably high altitudes. Examination of the data indicated that the measured MWIR temperatures were higher than those for nearby low clouds which were flagged as non-cirrus. A correction factor was developed and applied in these cases. After establishing the clear scene information, a maximum MWIR brightness temperature (after discarding the top 5%) for cloudy, non-cirrus pixels was calculated. This temperature is used to correct height assignments. Experiments showed that for cirrus pixels with a MWIR temperature higher than this maximum, the best approach to calculating optical properties was to treat them as low clouds.

The second set of problem conditions are a consequence of the pixel-level cloud property retrieval approach. Anomalies due to the variable cloud signatures can occur at cloud mass edges, the intersections of cloud masses of varying altitude, and near the day/night terminator. A correction was applied based on a moving 7x7 pixel frame centered on the pixel being analyzed. If a cirrus pixel is identified as being on an edge, i.e., clear and cirrus both found in the frame, then for retrieval purposes the pixel is treated as non-cirrus. Another correction applied was a check to see if the 3.7-μm brightness temperature of the pixel is within 6.5 K of the clear-column brightness temperature. If it is, the 10.7 μm emissivity is adjusted to be two thirds of the way between the retrieved emissivity and 1.0. Due to problems discriminating cirrus cloud near the

day-night boundary, terminator conditions resulted in far less consistent retrievals. Any pixels for which there was an anomalously high retrieved cloud altitude (> 17 km) were arbitrarily assigned values of 17 km. Our final results, represented by the over 700 cases analyzed provide the best data from which further characterization of these techniques can take place.

4.3.3 CIRRUS RETRIEVAL ACCURACY

Comparisons were made between SERCAA and coincident ground-based observations of cirrus cloud made over Wisconsin and Hanscom AFB during the 1995 SBIRS field experiment. Before discussing in detail the comparison results, it is first worthwhile to review differences in the data source platforms. SERCAA cirrus cloud top and optical depth analyses are provided at meteorological satellite sensor resolution, which is 1 km for AVHRR and 4 km for GOES-NEXT at nadir. CO_2 Slicing analyses are nominally 17 km for HIRS data, and 8 km for GOES-8. In contrast, coincident ground-based lidar and radar observations have spatial resolutions on the order of meters. In addition, there are significant differences between satellite imagers and ground-based radars/lidars in spectral bandwidths and band locations. Thus, some observing systems such as the lidars will be much more sensitive to highly transmissive cirrus than will be a passive infrared satellite radiometer. There are also time discrepancies and geolocation errors inherent in the multiple ground- and space-based data sources, although every effort was made to minimize these.

With all these factors in mind, the question arises of what is reasonable to expect for agreement when comparing such diverse analyses and observations. Although the SERCAA and lidar/radar comparisons are as quantitative as possible, comparisons cannot be performed in an absolute sense. In this light, comparisons were evaluated with one major theme in mind, namely, whether the observations dispute the satellite-based retrievals.

Visual comparison similar to those shown in Figures 10 and 11 between the cirrus retrievals, radar/lidar measurements, and blackbody retrievals were used to evaluate retrieval accuracy. Satellite-retrieval results were found to be consistent with ground- and aircraft-based observations of cirrus clouds for all cases tested. Retrieved emissivities are higher where the radar returns are stronger and vice versa. The cirrus altitude retrievals were found to be uniformly more accurate than the blackbody technique used by many cloud analysis models to compute cloud altitude for both opaque and transmissive clouds. Blackbody altitudes agree reasonably well with true cirrus altitudes wherever cirrus transmissivities are low (consistent with results in Figures 10 and 11). However, where cirrus is optically thin, the comparison

45

differences are dramatic. It is important to note that the blackbody technique is the approach used in the current Air Force operational global cloud analysis model, the RTNEPH, as well as in the Phase-I SERCAA algorithms being implemented as a part of CDFS-II.

Results obtained using GOES-8 6.7-μm water vapor image data in place of the 3.9-μm MWIR data show a bias of sorts in the water-vapor altitude retrievals that weights them much more closely to the true tops of the transmissive cirrus, in comparison to the respective MWIR retrievals. This bias is due primarily to the fact that in the cirrus environment there is more atmospheric water vapor than in the "clear-column" (i.e., cirrus-free) regions. The net result is that the 6.7-μm cirrus brightness temperature observations are more strongly influenced by this excess water vapor than are the corresponding 3.7-μm measurements, since the 3.7-μm spectral region is an atmospheric window wherein water-vapor absorption effects are minimal. There are two useful attributes to this deterministically explainable "bias." The first is that for the SBIRS program, cirrus cloud top altitudes are generally of more value than the "radiative center-of-mass" altitudes that the 3.7-μm data provide. The second is that in differencing the MWIR and water-vapor altitude retrievals, information on cirrus physical thickness that has been previously unobtainable using passive infrared retrieval techniques can now be inferred.

Comparisons were made between SERCAA altitude retrievals and the University of Wisconsin (UW) High Spectral Resolution Lidar (HSRL) near Madison, WI at 1915 UTC 4 August and 2315 UTC 7 September 1995. On 4 August, HSRL backscatter cross section (BCS) observations showed cirrus between 10 and 12 km. NOAA-14 AVHRR retrievals of the same cloud system fell within the same 10-12 km range, with the average cloud altitude at 11 km. As discussed above, the 11-km average altitude is more representative of the radiative center of mass of the cirrus clouds, and not the true tops. GOES-8 3.7-um retrievals for the same time fell in the 9-11 km range, with an average altitude of 10 km, all in all slightly lower than the AVHRR retrievals. The GOES 6.7-μm water-vapor retrievals show altitudes between 9 and 12 km, with an average altitude of 11 km. Note that the SERCAA water-vapor average altitude is 1 km higher than that obtained using the 3.7-μm data.

On 7 September, HSRL BCS observations indicated cirrus between 8 and 12 km. GOES-8 3.7-μm retrievals for the same time fell in the 9-10 km range, with an average altitude of 9.5 km. The GOES 6.7-μm water-vapor retrievals show altitudes between 10 and 11 km, with an average altitude of 10.5 km. Again the SERCAA water-vapor average altitude is 1 km higher than that obtained using the 3.7-μm data.

4.4 CLOUD RETRIEVAL COMPARISONS

The third and final task performed in support of the SBIRS PEP was a comparison between the modified SERCAA cirrus retrievals and coincident CO_2 slicing retrievals. In recent years CO_2 slicing has been extensively applied to both TIROS and GOES data to obtain cirrus emissivity and altitude statistics on a global scale (Wylie, Menzel, and Woolf, 1991; Menzel, Wylie, and Strabala, 1992). Satellite data cloud climatologies produced thus far using the CO_2 slicing method have been extensive, focusing on determining the geographical, seasonal, and diurnal changes of cloud cover (Wylie and Menzel, 1989). Previously, CO_2 slicing cloud analyses have been compared with lidar measurements and NWS ground-based cloud reports (Wylie and Menzel, 1989). Because of this legacy, the SBIRS PEP identified this technique to provide global information on the presence and characteristics of cirrus. To insure that these climatologies are representative of realworld conditions, a comparison study was performed between CO_2 slicing and the imager-based cloud retrievals described above.

During the 4-23 September 1996 SBIRS measurement campaign in southern Florida, coordinated measurements were made of cirrus clouds from polar orbiting and geosynchronous satellites, aircraft-mounted sensors, and ground-based radar and lidar platforms. These data were used as the basis for comparison of the two techniques. CO_2 slicing was applied to High-Resolution Infrared Sounder (HIRS) data and the modified SERCAA model analyzed data from the AVHRR sensor. Comparisons were made of cirrus cloud altitudes obtained for the same cloud scenes using measurements from the two independent sensors onboard the same NOAA TIROS polar orbiting satellites.

4.4.1 RELATIVE RETRIEVAL MODEL ATTRIBUTES

While the fundamental requirement is the same for both models, i.e. to detect the presence of thin cirrus and to determine its radiative and spatial attributes, the capabilities of the CO_2 slicing and imager-based techniques differ from each other in numerous respects. The most important differences between the two techniques are the respective spectral bands and spatial resolutions of the sounding and imaging sensors.

CO_2 slicing has been applied to both GOES VAS and NOAA HIRS sounder data. Using either data source, CO_2 can only resolve an effective emmissivity, defined as the product of the cloud fractional coverage N (within the sounder channel FOV) and the cloud emissivity ε. When applied to HIRS data, this FOV is large: nominally 227 km^2, corresponding to a 17-km diameter

at nadir. It is therefore to be expected that many HIRS FOVs are not uniformly cloud covered and contain large variations in cloud density. This has the effect of not allowing retrieval of the HIRS-derived cirrus emissivity alone; it is intrinsically tied to cirrus cloud fraction. Variation of cirrus properties within a HIRS FOV has a direct and (as of yet) partially untreatable consequence even on the post-analysis separability of cloud fraction N and emissivity ε from the effective emissivity $N\varepsilon$.

Like the CO_2 technique, the SERCAA approach only resolves an effective emissivity, and is therefore likewise sensitive to the effects of inter-pixel variability in cirrus optical properties. However, the high resolution AVHRR data used have a nominal FOV of 0.8 km^2, corresponding to a 1-km diameter. Hence, in comparison to HIRS pixels, an AVHRR FOV encompasses relatively small variations in cirrus cloud properties and, except near sharp cirrus edges, are frequently either entirely clear or entirely cloudy with a nearly constant emissivity. This predominantly dichotomous state of the cloud amount (N = 0 or 1) allows direct determination of cirrus bulk emissivity, i.e., cirrus bulk emissivity and cloud fraction are determined independently of each other.

For these reasons the direct comparison of SERCAA and CO_2 retrieved cirrus bulk emissivities is a complex process, beyond the limited scope of the intercomparison study performed here. However, cirrus effective altitudes are more directly comparable and, fortunately, of more direct interest to SBIRS.

4.4.2 DATA ANALYSTS AND COMPARISONS

AVHRR HRPT and coincident HIRS CO_2 sounder radiance data valid 4-23 September 1996 over the southeastern United States, the Gulf of Mexico, and the southwestern North Atlantic were analyzed for cirrus effective altitude. Figure 13 contains a frequency distribution of retrieved cirrus effective altitudes for the two independent analysis models. There is strong agreement between the altitude climatologies in the 7-to-13-km range. The largest differences between the two techniques is in the 5-to-7 and greater-than-13-km range bins. The SERCAA analyses show more clouds at lower altitudes, and CO_2 slicing shows more clouds at higher altitudes. At this point it is helpful to stratify these results into daytime and nighttime comparisons to better understand why these differences exist.
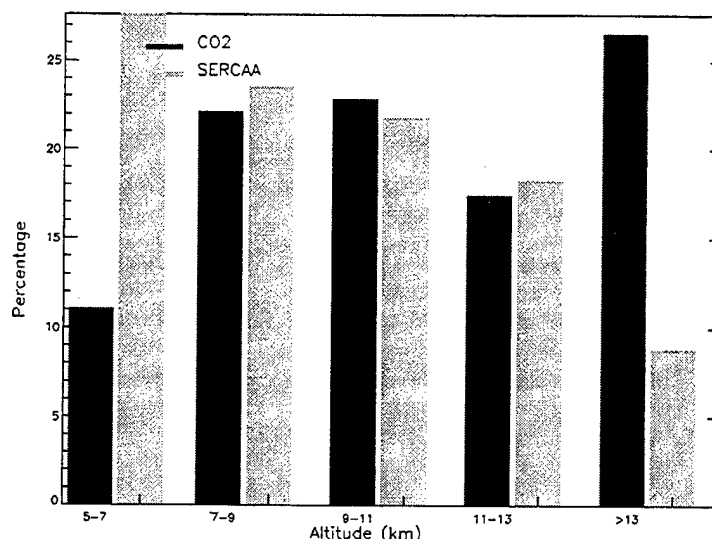
Figure 13 Frequency distribution of effective cirrus altitude for SERCAA and CO$_2$ Slicing

Figures 14 and 15 contain the daytime and nighttime effective-altitude frequency distributions, respectively. Note that the summary statistics show the same pattern both day and night: SERCAA analyzes more lower clouds and CO$_2$ Slicing analyzes more higher clouds. Thus, it is apparent that an algorithm diurnal bias of any sorts is not responsible for the overall lack of agreement in the very low and very high cirrus.

It is likely that the CO$_2$ slicing analyses are biased in a sense to false detection of high, thin cirrus. This is because in the CO$_2$ slicing analyses, otherwise clear-column edge-of-scan HIRS data are not explicitly corrected for increased atmospheric attenuation effects due to longer atmospheric path lengths. It is consequently suspected that the increased attenuation effects in clear-column HIRS pixels manifest themselves in the final analyses as very thin, very high clouds. That a high-cloud bias is evident both day and night lends credence to this hypothesis. There are two ways to study this thesis directly: 1) remove the edge-of-scan HIRS pixels from the intercomparisons between SERCAA and CO$_2$ Slicing effective altitudes (thus, only vertical-path 15-mm LWIR radiance will make their way into the final comparison statistics); 2) collocate each HIRS FOV with its many corresponding AVHRR FOVs and use the pixel-level SERCAA cloud/no-cloud analysis to determine whether the high-angle HIRS pixels are cloud-free. Each of these procedures is complex and requires more resources than this short-term study can support, however, these two ideas serve as sound issues to pursue in any follow-on studies.
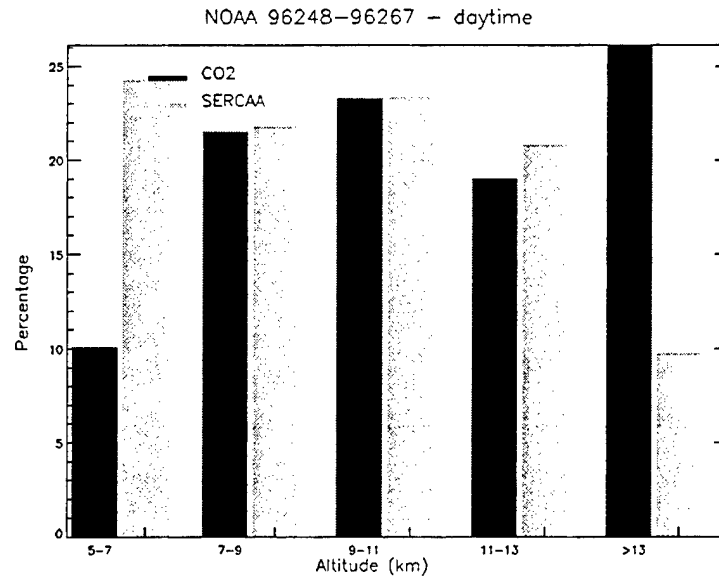
Figure 14 Daytime effective altitude frequency distributions
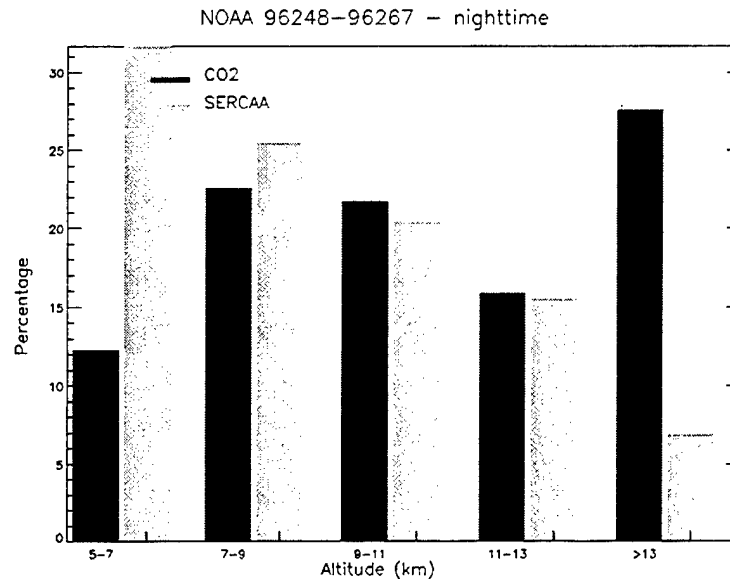
NOAA 96248-96267 — nighttime

Figure 15 Nighttime effective altitude frequency distributions

Aside from the high-cloud bias, there is one other interesting feature to note in the diurnal trends of the two analyses. Note that on average the analysis algorithms each detect fewer higher clouds than lower clouds at night. This agrees with more extensive cirrus climatologies of ocean regions (e.g., Wylie et al., 1989; Menzel, Wylie, and Strabala, 1992; Menzel, Wylie, and Strabala, 1993) over which this comparison study is a part.

4.5 SUMMARY

In support of the SBIRS Phenomenology Exploitation Project, SERCAA cloud analysis algorithms were expanded to include new and innovative multispectral infrared cirrus analysis techniques. These were successfully applied to two large data sets and compared to SBIRS cirrus detection, analysis, and ground-based observation scenarios. Integration of these and other retrieval techniques into the overall SERCAA cloud analysis allows the strongest and most reliable attributes of each technique to be combined into a single comprehensive cloud analysis product that more realistically represents cirrus spatial and optical properties than the current RTNEPH. With increasing amounts of multispectral infrared satellite data becoming available, the goal is to continue to retrieve from these data high quality augmented radiative, spatial, and microphysical properties of cirrus clouds in real-time and for climatological purposes at finer spatial and temporal resolution.

The effective altitudes obtained by the CO_2 slicing and SERCAA models compare well for the cirrus clouds observed during the 4-23 September 1996 field program centered over southeast Florida. The altitude summary statistics retrieved by the CO_2 slicing and SERCAA models agree with each other, after accounting for a high-cirrus bias evident in the CO_2 reports. The agreement between the two independent analyses of the same cirrus image scenes over a 20-day period provides an independent metric with which the accuracy of the more extensive CO_2 Slicing cirrus climatologies can be judged.

The CO_2 slicing and SERCAA models mutually complement each other. The SERCAA cirrus fraction N is useful to CO_2 slicing in separating the effect of N from the effective emissivity Nε for those cirrus clouds whose optical attributes are uniform within a particular HIRS FOV. This allows for direct comparisons of the true thermal infrared cirrus bulk emissivities retrieved by each technique. Spatial consistency can be determined by analyzing the AVHRR 3.7, 10.7 and 11.8 μm brightness temperature variations for cirrus clouds within a particular HIRS FOV. Such an expanded analysis will help to provide climate researchers with more physically realistic values of true cirrus emissivity from the climatologically extensive CO_2 slicing emissivities, free of any potentially compromising effects of cirrus cloud fraction. On the other hand, the CO_2 slicing technique provides an independent determination of cirrus effective altitude which obviates the need for the SERCAA parameterization of the variation of ε with wavelength, as required by Eq. (8). In an automated sense the CO_2 slicing and SERCAA cirrus

51

models can be used together to increase the accuracy of the retrieved cirrus parameters. SERCAA can support the CO_2 slicing method in determining the temperature (radiance) of the surface underlying any transmissive cirrus. This may be either the clear ground or an underlying liquid water cloud. Improved estimates of underlying cloud or surface temperature can significantly improve the CO_2 slicing determination of cirrus bulk emissivity. Better cirrus emissivity climatologies in turn will significantly improve the accuracy of radiative models used in climate and global change studies.

5.0 CONTRAIL EXPERIMENT SUPPORT

An extensive data collection campaign was conducted between 18-29 September 1995 as part of a PL/GPA sponsored contrail experiment designed to develop and improve contrail prediction and forecast capabilities. Program objectives are: 1) to determine the vertical and horizontal extent of water vapor from 300-700 mb using an extensive network of airborne, space-based and land-based sensors; 2) test and verify variations of Appleman's equation for contrail formation using real-time data; and 3) use the regional MM5 forecast model to attempt to accurately forecast contrail formation through upper-level moisture enhancements. Ground-based TPQ-11 radar data, satellite observations, and standard 0000 and 1200 UTC upper air NWS soundings were collected in the vicinity of Hanscom AFB on a daily basis. In addition, a series of radiosonde releases from five surrounding locations was conducted to provide a data rich environment of upper air observations over the contrail experiment area. Radiosonde launches occurred approximately every three hours during daylight hours. The five stations that made up the local radiosonde network were: Hanscom AFB, Beverly, UMASS Lowell, Otis AFB, and Chatham on Cape Cod.

The radiosonde data reduction effort was complicated by numerous problems and inconsistencies with the radiosonde measurements that needed to be resolved in order to produce a useful data set. Record books of balloon-flight problems, cloud types and heights as well as technical problems and observations of actual aircraft contrails were used to help classify problems. All radiosonde measurements were subjected to an extensive quality control procedure to identify and remove invalid data. All QC processing was performed manually using a spread sheet program to store and manipulate the data and graphical representations to identify problems in the data set.

5.1 DATA PROBLEMS

Radiosonde data from Otis and Hanscom proved to be the most reliable and accurate when pressure, temperature, and RH values were checked against nearby NWS radiosonde sites and other independent data. Significant problems were evident in the data from the UMASS Lowell site and especially the Beverly observations. Two different manufacturers were used to supply radiosondes for the measurement campaign; VIZ and Vaisala. Throughout the data collection period sondes from the two sources were found to have different sensitivities to relative humidity (RH). The RH of the Vaisala sondes generally ranged between 0 and 80% with very large

negative RH values occurring above 400 mb. VIZ sondes tended to be much less sensitive with RH values typically ranging between 20% and 60%. Even when synoptic observations and other supporting meteorological data which confirmed RH values near 100%, VIZ sondes rarely exceeded 60% RH.

Beverly sounding data were more noisy relative to the other four sites due to less sensitive receiving equipment and proximity of the site to the FAA tower at Beverly Airport. RF transmitting equipment in the FAA towers severely degraded the quality of signal received by the radiosonde ground system. The parameter most affected was pressure. Contaminated pressure soundings exhibited sinusoidal variations of 0.0 to 0.5 mb about what would be a typical pressure sounding. Thus, the pressure data were smoothed using a running average computed over the six data points above and below the target data point. The smoothing successfully removed the sinusoidal variations.

Because of the proximity of the UMASS Lowell and Beverly sites and identical release times, some cross-talk occurred from the UMASS radiosonde at the Beverly site. During several of the launches, the UMASS sonde was tracked at the Beverly site. On other occasions the Beverly receiver lock would switch back and forth from the UMASS radiosonde to the Beverly sonde during the tracking period. Difficulty in determining the accuracy and validity of the Beverly measurements when these switchovers occurred was common.

Additional processing for the Chatham soundings was also needed to account for incorrect computation of relative humidity, especially at low (<20%) and high (>95%) humidity values.

5.2   RESOLUTION OF RADIOSONDE PROBLEMS

Figures 16 and 17 represents typical pressure related problems with the Beverly data. Note the constant pressure trace at the beginning of the record (left side of Figure 16). Approximately the first 900 seconds of data collection occurred before balloon release while the sonde was held on the ground (a common problem). These times were truncated and the start times reestablished from the actual release time. Also observable in Figures 16 and 17 are outlying pressure data points. These were a common occurrence and needed to be manually removed from the data. Pressure data were then smoothed using a running average of six data points above and below each data point. The radiosonde sounding from Beverly shown in Figure 17 also shows the impact of the UMASS Lowell radiosonde on Beverly's tracking. Near 800 mb and again between 300 and 200 mb contact with the Beverly sonde is lost and the UMASS Lowell sonde is

picked up in its place. Soundings of this type were either totally or partially discarded if the data could not be verified as originating from the Beverly sonde.
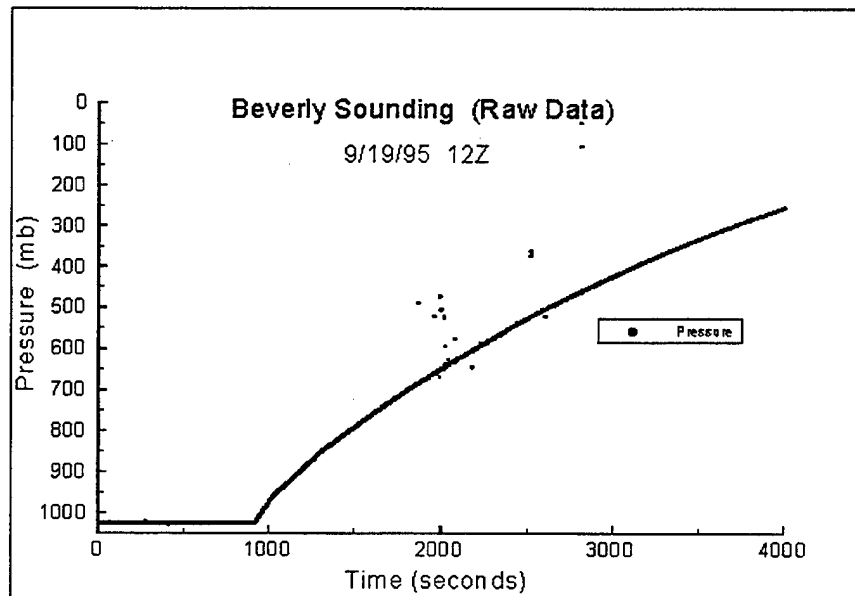

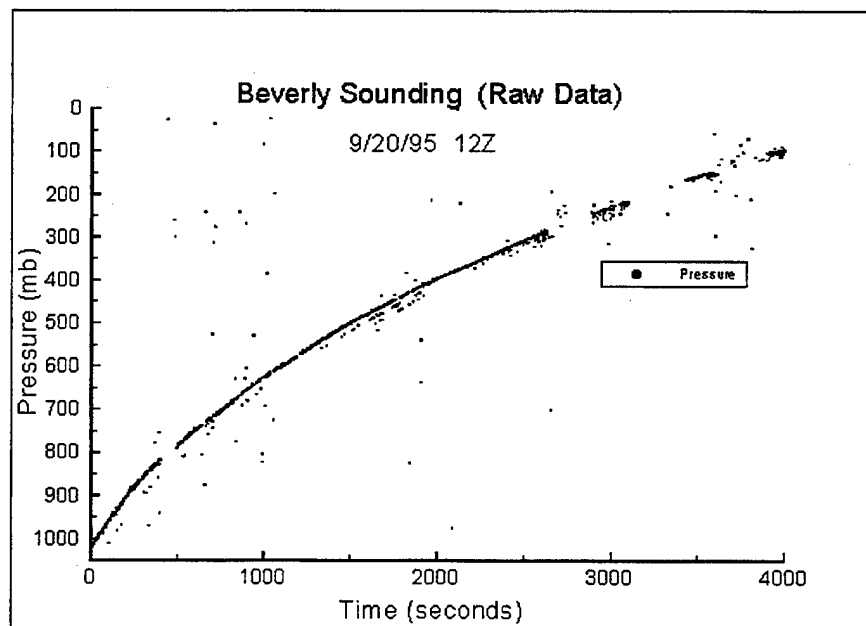**Figure 16 Pressure trace from Beverly sounding at 1200 UTC on 19Sep95.**

Figure 17 Pressure trace from Beverly sounding at 1200 UTC on 20Sep95

Relative humidity proved to be equally difficult to quality control as RH values fluctuated greatly over short periods of time, uncharacteristic of actual atmospheric conditions.   Large spikes of both positive and negative RH values above 300 mb were common.   The Beverly data

shown in Figure 18 illustrates a typical RH profile. Outlying relative humidity values and fluctuations over short periods were manually removed and negative values set to either 0 or missing (-999). RH values were then smoothed using the six-point running average technique described above.
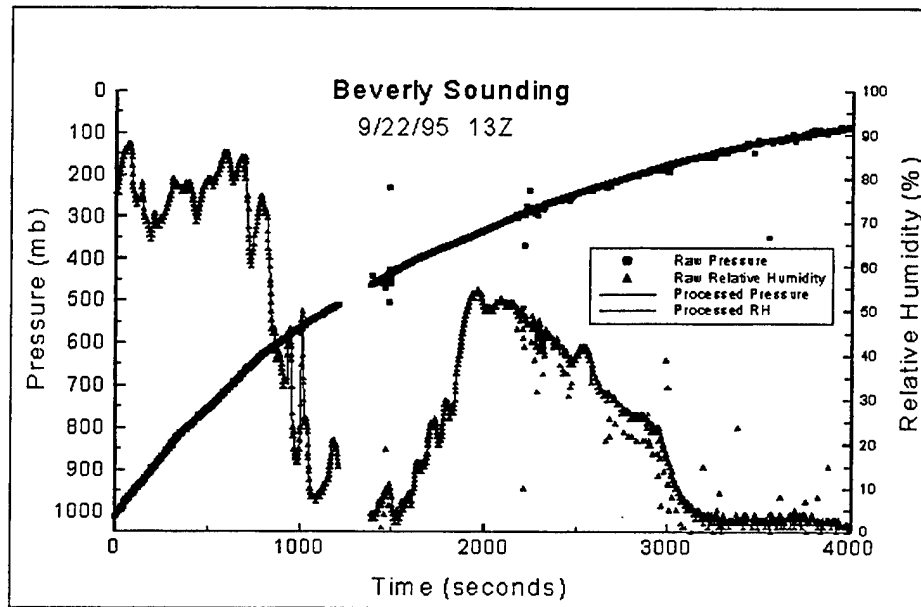

Figure 18 Pressure (smooth curve monotonically increasing from left to right) and relative humidity traces from Beverly sounding at 1300 UTC on 22Sep95

Some sites such as Beverly provided a limited data set consisting only of pressure, temperature and relative humidity. Other sites also provided dew point, corrected RH, wind speed and direction. A common data base was required for the project, so limited data sets were augmented, where possible, with derived parameters to fill in the missing quantities. Required parameters were: time since launch, pressure, geopotential height, air temperature, dew point temperature, relative humidity, corrected relative humidity, wind speed, wind direction, and distance from launch point. Finally, tropopause height was estimated by manually by: 1) determining the level of minimum temperature; 2) identifying an isothermal layer above; and 3) noting a decrease in wind speed with height. A determination of tropopause thickness was also made where data permitted. Table 15 is an excerpt from a complete and corrected sounding.

Table 15 Sample sounding data from Chatham at 1200 UTC 18Sep95, after reformatting and quality control processing

TIME (s)	P (mb)	HT (m)	T (C)	Td (C)	RH (%)	RHc (%)	SPD (m/s)	DIR	X (km)	Y (km)
636	732.8	2675	6.3	-8.4	45.2	0	13.8	296	3.01	-4.96
642	730.6	2700	6.1	-8.3	45.9	0	13.9	295	3.09	-5
648	728.4	2724	5.8	-8.3	46.7	0	14	295	3.17	-5.03
654	726.1	2750	5.6	-7.6	49.1	0	14	294	3.24	-5.07
660	723.9	2775	5.3	-7.6	49.8	0	14	293	3.32	-5.1
666	721.4	2803	5.1	-7.6	50.4	0	14	292	3.4	-5.13
672	719	2830	5	-8.1	49.1	0	13.9	292	3.48	-5.16
678	716.6	2858	4.9	-8.5	48.3	0	13.7	291	3.55	-5.19
684	714.2	2885	4.7	-9.8	45.3	0	13.5	291	3.63	-5.22
690	711.9	2911	4.6	-9.9	45.2	0	13.2	290	3.7	-5.25
696	709.6	2938	4.4	-11.1	42.6	0	12.9	290	3.77	-5.27
702	707.4	2963	4.6	-24.9	19	-0.9	12.6	289	3.85	-5.3
708	705.1	2989	4.8	-75.2	14	-13.7	12.3	289	3.92	-5.32
714	702.9	3015	5	-85.4	11.4	-11.3	12	289	3.98	-5.35
720	700.8	3039	5.2	-85.3	10.9	-10.8	11.7	288	4.05	-5.37
726	698.7	3064	5.4	-85.2	9.9	-9.8	11.5	288	4.12	-5.39
732	696.6	3088	5.6	-85.2	9.2	-9.1	11.3	287	4.18	-5.41
738	694.5	3113	5.8	-85.1	9.3	-9.2	11.1	287	4.25	-5.43
744	692.4	3138	6	-85	9.2	-9.1	10.9	287	4.31	-5.45
750	690.2	3164	6.2	-84.9	9.3	-9.2	10.8	286	4.37	-5.46

5.3   SUMMARY

Radiosonde data collected as part of the PL/GPA Contrail Experiment required considerable manual quality control and editing as part of the data reduction process. This process is summarized in the steps below:

1) all soundings were edited by manual inspection to remove obviously incorrect data and replace them with a missing designation;

2) additional editing of Beverly radiosonde measurements, particularly the pressure and relative humidity parameters, was required to address noisy data caused by less sensitive ground-receiving equipment and the proximity of site to the FAA control tower;

3) additional processing for Chatham soundings was needed to correct for unrealistic relative humidity extremes;

4) missing layers were noted;

5) corrections for launch times were made;

6) vertical coverage of each sounding was recorded;

7) a subjective quality assessment for each sounding was recorded (e.g., was the correct radiosonde being tracked during the flight);

8) each sounding tagged by the sonde manufacturer, either VIZ or Vaisala;

9) tropopause height and thickness were determined if possible;

10) a common format for all radiosonde soundings was established and missing parameters calculated; and

11) all radiosonde data archived in a common format to facilitate future processing.

6.0 REFERENCES

Barton, I. J., 1983: Upper Level Cloud Climatology from an Orbiting Satellite. Journ. Atmos. Sci., 40, 435 - 447.

d'Entremont, R. P., D. P. Wylie, S.-C. Ou, and K.-N. Liou, 1996: Retrieval of Cirrus Radiative and Spatial Properties Using Coincident Multispectral Imager and Sounder Data. Preprints, Eighth Conf. On Satellite Meteorology and Oceanography, Amer. Meteor. Soc., Atlanta, GA, 28 January - 2 February 1996, 377 - 381.

Gustafson, G.B., R.G. Isaacs, R.P. d'Entremont, J.M. Sparrow, T.M. Hamill, C. Grassotti, D.W. Johnson, C.P. Sarkisian, D.C. Peduzzi, B.T. Pearson, V.D. Jakabhazy, J.S. gelfiore, and A.S. Lisa, 1994: Support of Environmental Requirements for Cloud Analysis and Archive (SERCAA): Algorithm Descriptions. PL-TR-94-2114, Phillips Laboratory, Hanscom AFB, MA, ADA 283240.

Hoke, J.E., J.L. Hayes, L.G. Renninger, 1981: Map projections and grid systems for meteorological applications. AFGWC-TN-79-003, Air Weather Service, Scot AFB, IL.

Hunt, Garry E., 1973: Radiative Properties of Terrestrial Clouds at Visible and Infra-Red Thermal Window Wavelengths. Quart. Journ. Royal Meteor. Soc., 99, 346 - 369.

Menzel, W. P., Donald P. Wylie, and K. I. Strabala, 1993: Trends in Global Cirrus Inferred From Three Years of HIRS Data. Seventh Int'l. TOVS Conference, Austria, 10-16 February 1993.

Menzel, W. P., Donald P. Wylie, and Katherine. I. Strabala, 1992: Seasonal and Diurnal Changes in Cirrus Clouds as Seen in Four Years of Observations with the VAS. Journ. Appl. Meteor., 31, 370 - 385.

Ou, S. C., K. N. Liou, W. M. Gooch, and Y. Takano, 1993: Remote Sensing of Cirrus Cloud Parameters Using Advanced Very High Resolution Radiometer 3.7- and 10.9-,um Channels. Appl. Optics, 32, 2171-2180.

Schiffer, R. A., and W. B. Rossow, 1983: The International Satellite Cloud Climatology Project (ISCCP): the First Project of the World Climate Research Programme. Bull. Amer. Meteor. Soc., 64, 779 - 784.

Smith, W. L., H. E. Revercomb, H. B. Howell, and M.-X. Lin, 1990: Multi-spectral Window Radiance Observations of Cirrus From Satellite and Aircraft, November 2, 1986 Project FIRE. FIRE Science Results 1988, NASA Langley Res. Ctr., 89 - 93.

Takano, Y., and K. N. Liou, 1989: Solar Radiative Transfer in Cirrus Clouds. Part I: Single Scattering and Optical Properties of Hexagonal Ice Crystals. Journ. Atmos. Sci., 46, 3 -19.

Woodbury, G. E., and M. P. McCormick, 1983: Global Distribution of Cirrus Clouds Determined from SAGE Data. Geophys. Res. Lett., 10, 1180 - 1183.

Wylie, Donald P., and W. P. Menzel, 1989: Two Years of Cloud Cover Statistics Using VAS. Journ. of Clim., 2, 380 - 392.